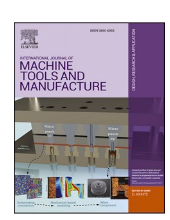
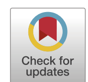
International Journal of Machine Tools & Manufacture 190 (2023) 104048

Contents lists available at ScienceDirect

International Journal of Machine Tools and Manufacture

journal homepage: www.elsevier.com/locate/ijmactool





Investigation of the low-frequency chatter in robotic milling

Shihao Xin [a], Xiaowei Tang [a,*], Jiawei Wu [a], Fangyu Peng [a,b], Rong Yan [a], Wei Yang [a]

[a] School of Mechanical Science and Engineering, Huazhong University of Science and Technology, Wuhan, 430074, China
[b] State Key Laboratory of Digital Manufacturing Equipment and Technology, Huazhong University of Science and Technology, Wuhan, 430074, China

ARTICLE INFO

Handling Editor: Dragos Axinte

Keywords:
Robotic milling
Low-frequency chatter
Mode coupling effect
Regenerative effect
Modulated tool-workpiece engagement conditions

ABSTRACT

In robotic milling with large allowance process, low-frequency chatter (LFC) is an important factor observed in high-speed and low-speed milling, affecting the processing efficiency and quality. Previous research has used the regenerative chatter theory, ignoring modulated tool-workpiece engagement conditions, or mode coupling theory under the assumption of threading operations to explain the LFC mechanism and predict the stability boundary. However, these models overlook or inaccurately characterize the modulation effect, leading to inaccurate modeling of dynamic chip thickness changes during milling, making it difficult to understand the mechanism of LFC. Here, we propose an LFC stability model that considers modulated tool-workpiece engagement conditions and the mode coupling effect of the robotic structure for robotic milling. This approach allows us to reveal the mechanism of LFC and identify the characteristic signal of low-frequency vibration, which is the sideband frequency signal. Initially, the evolution of LFC is analyzed, and its characteristics are summarized. Further, a surface renewal (SR) model is proposed to accurately calculate the dynamic cutting force caused by modulated tool-workpiece engagement conditions in LFC. Furthermore, the LFC stability model, considering the modulated tool-workpiece engagement conditions and mode coupling effect, is established based on impulse response function (IRF) method. Finally, we verify the accuracy of our model through milling experiments and compare it with that of the classical stability prediction model. Our results show that LFC is highly dependent on speed, and our stability model can effectively predict the stability boundary of LFC in robotic milling with large allowance process.

1. Introduction

Chatter diminishes the quality and efficiency in robotic milling [1]. Majority of research on chatter in robotic milling mainly includes high-frequency chatter, dominated by the tool mode [2], and low-frequency chatter (LFC), dominated by the robotic structural mode [3]. In conventional machining systems, the stiffness of the machine tool is typically higher than that of the tool structure. Thus, research mainly focuses on high-frequency chatter dominated by the tool mode, and structural modes of machine tools are only considered in heavy-duty low-speed machining where the chatter mechanism is similar to regenerative chatter. However, in robotic milling, the stiffness of the robot structure is lower than that of the tool structure; LFC dominated by the robot structural mode cannot be overlooked, particularly in heavy-duty machining where low-frequency modes are more likely to be excited, and LFC is often observed. This phenomenon is a critical difference between robotic milling and machine tool milling. High-frequency chatter is mostly explained by regenerative effect [4], while LFC demonstration involves two models based on mode coupling effect [5] and regenerative effect [6].

Many researchers have conducted studies on the regenerative effect of machine tool milling stability theory to address high-frequency chatter in robotic milling. For example, Tunc et al. [2] considered the impact of asymmetric dynamic compliance related to robotic position on tool tip dynamic characteristics and developed a regenerative chatter stability model that relies on machining position and feed direction. Chen et al. [7] proposed a method for predicting the frequency response of the tool tip dependent on robotic posture, using the inverse distance weighting method. By combining the regenerative chatter model, the authors achieved stability prediction of robotic milling. Cordes et al. [8] studied the dominant mode of regenerative chatter stability in robot milling at high (5000–30000 rpm) and low speeds (100–1100 rpm), as well as verified the accuracy of their stability prediction through milling experiments with different materials. Mousavi [9] et al. investigated how to optimize the milling stability concerning robotic posture by

* Corresponding author.
E-mail addresses: shxin@hust.edu.cn (S. Xin), tangxw@hust.edu.cn (X. Tang), d202080296@hust.edu.cn (J. Wu), pengfy@hust.edu.cn (F. Peng), yanrong@hust.edu.cn (R. Yan), ywwh@hust.edu.cn (W. Yang).

https://doi.org/10.1016/j.ijmachtools.2023.104048
Received 6 February 2023; Received in revised form 5 June 2023; Accepted 7 June 2023
Available online 15 June 2023

Nomenclature

Lobe order　the ratio between such natural frequency and the tooth passing frequency
$X(t)$　the tool path at time t
$X(t\text{-}\tau_0)$　the tool path at time $t\text{-}\tau_0$
τ_0　delay time
$h_b(t)$　instantaneous chip thickness of threading operation
$h_m(t)$　instantaneous chip thickness of milling
$h_{b0}(t)$　nominal chip thickness of threading operation
$h_{m0}(t)$　nominal chip thickness of milling
$\delta h_b(t)$　dynamic chip thickness of threading operation
$\delta h_m(t)$　dynamic chip thickness of milling
$y_{bd}(t)$　vibration in the Y direction of threading operation at time t
$x_{md}(t)$　vibration in the X direction of milling at time t
$y_{md}(t)$　vibration in the Y direction of milling at time t
$x_{md}(t\text{-}\tau_0)$　vibration in the X direction of milling at time $t\text{-}\tau_0$
$y_{md}(t\text{-}\tau_0)$　vibration in the Y direction of milling at time $t\text{-}\tau_0$
f_c　chatter frequency
f_{tp}　tooth passing frequency
T_c　chatter period in critical stable state
T_{tp}　tooth passing period
N　number of teeth
n　spindle speed
$d(t)$　the vibration at time t
$d(t\text{-}T_{tp})$　the vibration at time $t\text{-}T_{tp}$
A　cutting point
B　blade point
R　tool radius
$x_{lev,ij}(t)$　additional vibration displacement (X-direction) caused by low-frequency chatter at time t
$y_{lev,ij}(t)$　additional vibration displacement (Y-direction) caused by low-frequency chatter at time t
$\varphi_{ij}(t)$　immersion angle at time t
i　the number of cutting elements
j　teeth number of the tool
$x_{T,ij}(t)$　the x coordinate at point B at time t
$y_{T,ij}(t)$　the y coordinate at point B at time t
$x_{T,ij,n}(t)$　the x coordinate at point A at time t
$y_{T,ij,n}(t)$　the y coordinate at point A at time t
f　feed speed
$\varphi_{T,ij,n}(t)$　the angle between OA and feed direction
$h_{ij}(t_2)$　instantaneous chip thickness at time t_2
$h_{ij}(t_3)$　instantaneous chip thickness at time t_3
$g_{ij}(t)$　unit step function to judge whether cutting occurs
$F_x(t)$　instantaneous cutting force in the X direction
$F_y(t)$　instantaneous cutting force in the Y direction
$F_z(t)$　instantaneous cutting force in the Z direction
k_{tc}, k_{rc}, k_{ac}　cutting force coefficient
α_{ij}　axial contact angle
$X(\omega)$, $Y(\omega)$, $Z(\omega)$　vibration of the robot end in the X, Y, and Z directions
$\mathbf{H}_{ij}$　FRFs of the robot end in the i direction responding to the excitation in the j direction
$\mathbf{F}_i(\omega)$　cutting force on the robot end in i direction
m　modal order
$M_{n,ij}$　the modal mass of each order in each direction
$C_{n,ij}$　the modal damping of each order in each direction
$K_{n,ij}$　the modal stiffness of each order in each direction
X_{xn}, X_{yn}, X_{zn}　the vibration displacement response of each mode in the X direction caused by the cutting forces in the X, Y and Z directions
$X(k\tau+\tau)$　the response of the system at $k+1$ in the X direction
τ　discrete time
k　number of iterations
f_{ij}　unit IRF within a given bandwidth, the subscripts i and j represent the response in the i-direction caused by the excitation in the j-direction
f_z　feed per tooth
t_{st}　the time to start recording simulation results
t_{ex}　the time to finish recording simulation results
CI_{ER}　Energy Ratio Chatter Indicator
E　energy of the vibration signal
E_c　energy of the aperiodic component of the vibration signal caused by chatter
E_p　energy of the periodic component of the vibration signal
E_n　energy of the aperiodic component caused by environmental noise
a_p　axial cutting depth
dz　differential element thickness
$h(\varphi_{ij})$　instantaneous cutting thickness without considering dynamic chip thickness
$\widetilde{h}(\varphi_{ij})$instantaneous cutting thickness with considering dynamic chip thickness$M$　instantaneous cutting thickness with considering dynamic chip thickness$M$number of differential elements of axial cutting depth
ΔX, ΔY, ΔZ　dynamic change in the X, Y and Z directions
ΔF_x, ΔF_y, ΔF_z　dynamic cutting force in the X, Y and Z directions
$\widetilde{M}$dynamic change of the number of differential elementsLFC　dynamic change of the number of differential elementsLFClow-frequency chatter
SR　surface renewal
IRF　impulse response function
IDW　inverse distance weighting
FDM　full-discretization method
CCT　conservative congruence transformation
IUCT　instantaneous uncut chip thickness
MFA　Multi frequency approximation

predicting the stability boundary of each redundant degree of freedom (DOF) in the robotic machining trajectory, allowing stability optimization without changing the cutting parameters. Similarly, Gonul et al. [10] studied the influence of robotic redundant DOF on tool tip frequency response in the feed direction and realized stability optimization related to the feed direction based on the regenerative chatter stability model. These studies focus primarily on regenerative chatter dominated by the tool structure mode. The regenerative chatter mechanism is the same as that of the machine tool, but the dynamic characteristics of the tool can be changed through posture changes [11–13]. Additionally, it is important to note that in the conducted chatter experiments, only high-frequency signals related to the tool mode are monitored. The research on high-frequency chatter dominated by the tool structure mode in robotic milling has attained a relatively mature stage and can serve as a helpful guideline for optimizing cutting parameters in cases where chatter is also dominated by the tool structure mode. It should be noted that in the regenerative chatter mechanism described above, the tooth-passing frequency is much lower than the chatter frequency, which can range from hundreds to thousands of hertz. The lobe order, defined as the ratio between the natural frequency and the tooth-passing frequency [14], is greater than 1, resulting in a tool-workpiece engagement state with a period smaller than the tooth-passing period. Therefore, using stability prediction results within a tooth-passing period is a reasonable way to characterize the stability of the

machining process.

However, in cases where large allowance processing is required, a larger tool is typically used. At this point, the tool's stiffness is much greater than that of the robotic structure, making the influence of the low-frequency mode of the robotic structure a dominant factor in stability analysis. To study and explain LFC in robotic milling, some scholars have applied the regenerative effect mechanism derived from machine tool chatter, which is typically used for high-frequency chatter prediction. For instance, Tunc et al. [6] used the regenerative chatter model of CNC milling and introduced the low-frequency mode of the robot to calculate the LFC stability boundary of robotic milling. Cordes et al. [8] analyzed the stability of the robotic milling system using the semi-discrete time domain method. In their study, they discovered that the pose-dependency modes of the robot structure were all low-frequency; this mode produced LFC during low-speed milling of titanium parts. Cordes et al. [8] also predicted the LFC stability boundary dominated by the robotic low-frequency modes, as shown in Fig. 1a, where modes 1, 2 and modes 3, 4 represent the LFC stability boundary dominated by the robotic structural modes. Similarly, Tunc et al. [6] investigated LFC and the predicted results are shown in Fig. 1b. Xin et al. [13] used the full-discretization method (FDM) to predict the stability boundary of LFC, as demonstrated in Fig. 1c.

Notably, LFC in robotic milling typically occurs in tens of hertz range. For example, the robot used in this study has a structural modal frequency range of 10–30 Hz, whereas a range of 10–26 Hz was observed in Refs. [6,8,13]. The natural frequency of the robot structure mode is much lower than that of the tool mode, which is typically in hundreds or thousands of hertz range in high-frequency chatter [2,9,10]. Due to the extremely low natural frequency of the robot structure mode, the lobe order is typically lower than unity. It should be noted that when considering multiple modes, the lobe order should be determined by the first mode. When the lobe order is less than 1, there are multiple tooth-passing periods in a single dynamic chip thickness period, and conversely, multiple dynamic chip thickness periods in a single tooth-passing period (Considering the tooth passing frequency of 200 Hz generated by a 4-tooth cutter with a common spindle speed of 3000 rpm as an example, lobe order was much lower than 1 for low-frequency chatter, but much higher than 1 for high frequency chatter). The multiple dynamic chip thickness periods cause significant differences in the tool-workpiece engagement conditions, which can yield different dynamic chip thickness characteristics and require different modeling and solving approaches for the regenerative effect (see Section 2.3 for a more detailed analysis). These special tool-workpiece engagement conditions, which are induced when the lobe order is less than unity, are referred to as modulated tool-workpiece engagement conditions.

Despite the use of regenerative chatter theory derived from machine tool chatter can be used to predict the stability border for the LFC of robotic milling, as shown in Fig. 1, the applicable spindle speed range (lobe order $\geq$1) is significantly reduced to satisfy the condition that a tooth-passing period consists of multiple chatter periods, which is the existing mechanism of regenerative effect chatter. However, in the higher spindle speed range where the lobe order $<$1 and a dynamic chip thickness period consists of multiple tooth-passing periods, the stability boundary exhibits an infinite increase trend, which is not consistent with the actual situation. Our robot machining experiments have also demonstrated that the limit cutting depth of stability does not increase infinitely when machining at higher spindle speeds. Therefore, to expand the applicability of the mechanism of regenerative effect in the higher spindle speed ranges of robotic milling where the lobe order is less than unity, further investigation of the mechanism of regenerative effect with modulated tool-workpiece engagement conditions is required based on the existing research on the regenerative effect.

One approach to studying LFC in robotic milling is to consider the mode coupling effect [15,16]. In 2006, Pan et al. [3], explained the mechanism, established the model, and predicted the LFC stability in robotic milling based on the mode coupling effect. A 2-degree-of-freedom (2-DOF) mode coupling dynamic model was established. Its stability prediction results showed that the stability limit of the robot considering mode coupling chatter depends on the angle between the machining force vector and the main stiffness direction. The stability prediction results are shown in Fig. 2d. Cen et al. [17,18] further improved the model by projecting the cutting force in the robotic stiffness direction by rotating the coordinate system. A conservative congruence transformation stiffness model was applied to correlate robotic stiffness in Cartesian space with joint space, which included the effect of milling forces on robotic stiffness in the stability model. They provided a stability boundary diagram, as shown in Fig. 2b. System stability is related to the angle γ between the direction of the resultant force and that of principal stiffness. Wang et al. [19] studied the reliability of mode coupling chatter in robotic milling and identified the reliability and unreliability regions of mode coupling chatter by establishing the mode coupling chatter probability model. The mode coupling

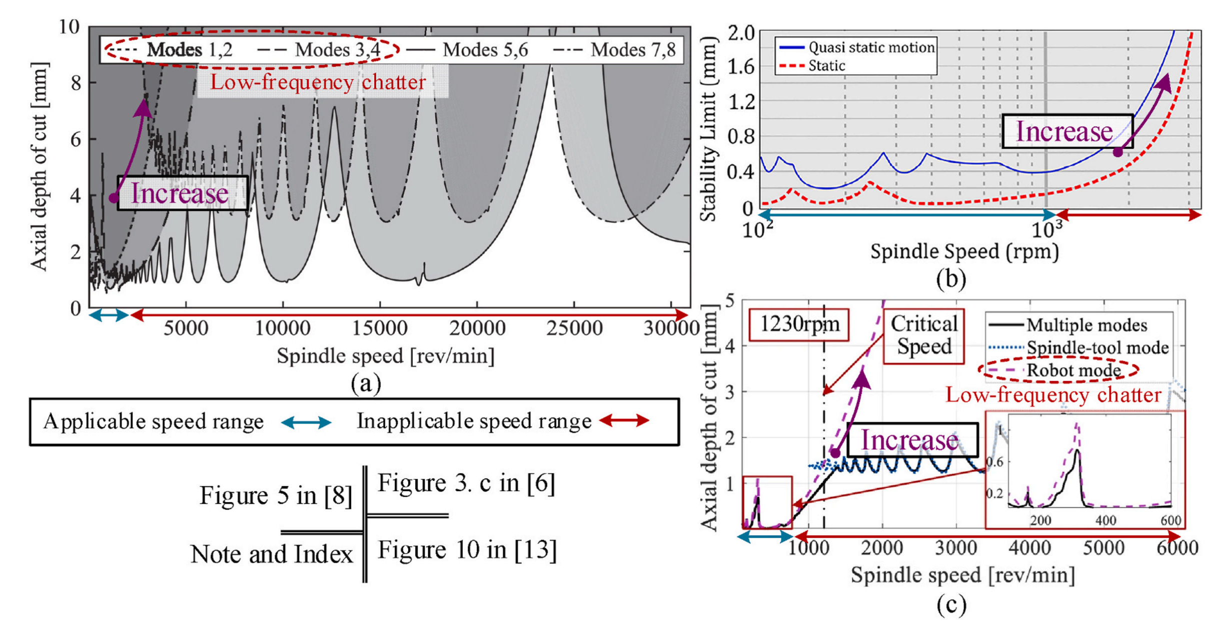


Fig. 1. Stability lobe diagram of low-frequency chatter model based on regenerative effect. (a) Fig. 5 in Ref. [8], (b) Fig. 3 in Ref. [6], (c) Fig. 10 in Ref. [13].

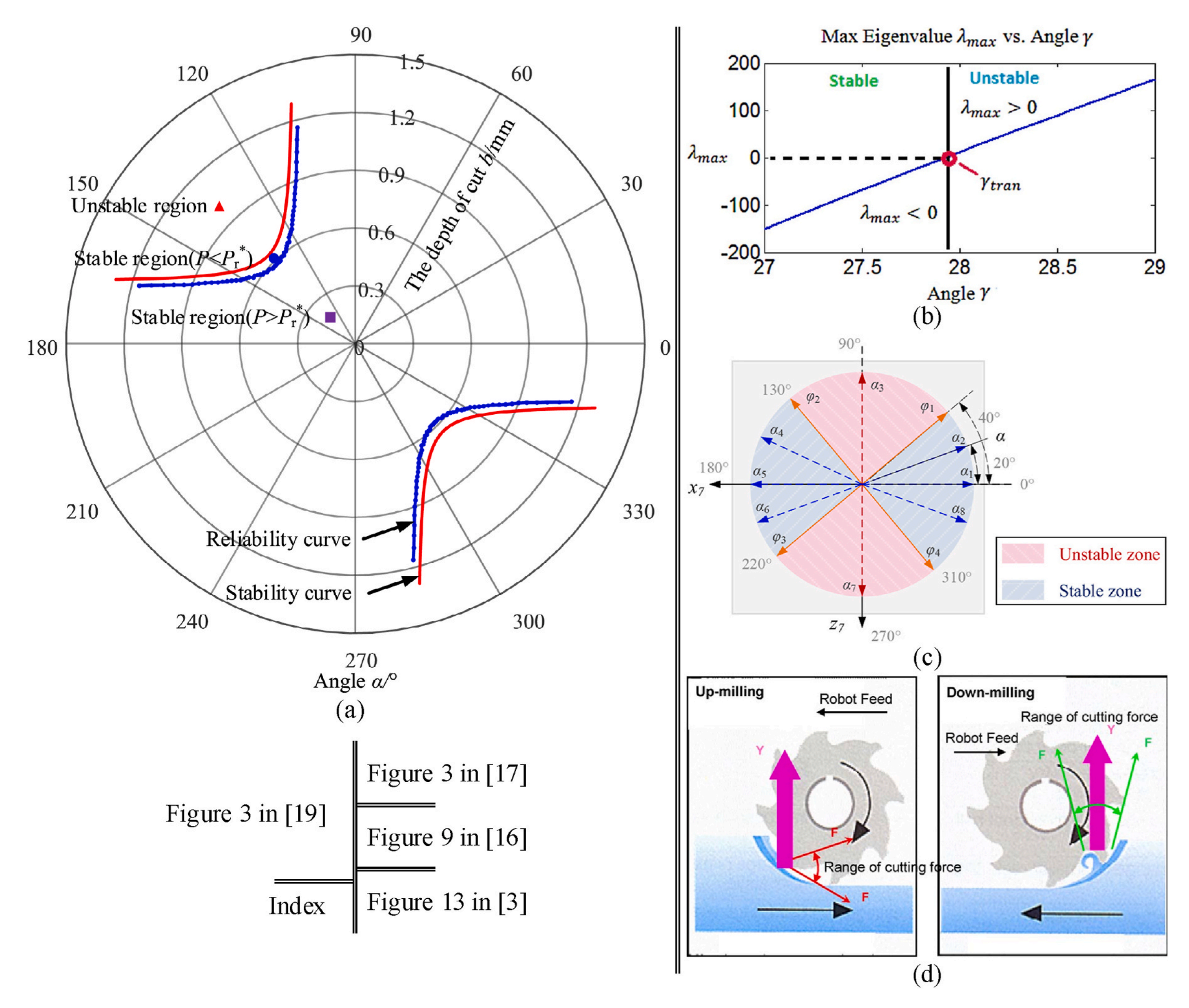


Fig. 2. Stability boundary diagram of low-frequency chatter model based on mode coupling effect. (a) Fig. 3 in Ref. [19], (b) Fig. 3 in Ref. [17], (c) Fig. 9 in Ref. [16], (d) Fig. 13 in Ref. [3].

chatter reliability circle diagram was provided, as shown in Fig. 2a. In addition, Liu et al. [20] measured the accuracy of mode coupling chatter stability prediction using reliability theory. Gienke et al. [5] proposed an extended mode coupling chatter theory suitable for robotic kinematics. He et al. [16] established a 3-DOF stability model of robotic milling and obtained a 3-dimensional criterion of mode coupling chatter. The stability of the system is related to the feed direction, and the stability circle diagram is shown in Fig. 2c. On the other hand, several scholars have investigated the factors that influence mode coupling chatter through milling experiments. For instance, Li et al. [12] analyzed the tool trajectory and workpiece clamping position, while Maulimov et al. [21] and Liu et al. [22] studied the tool feed direction as well as spindle speed, tool overhang length, axial depth of cut, feed rate, and cutting material, respectively. While the mode coupling effect can explain the occurrence of LFC to a certain extent, most of the existing models are based on threading operations, which characterize processing stability by adopting the angle between the resultant force and the direction of the principal stiffness. This approach makes two assumptions: first, that the average cutting force coefficient is sufficient to ignore the dynamic change of cutting force direction, and second, that the dynamic cutting force is only related to the current vibration and not influenced by the previous chip wave on the dynamic chip thickness. As a result, the time delay term in the dynamic equation is ignored, and the tool-workpiece engagement conditions in milling are not accurately characterized, especially for the modulated tool-workpiece engagement conditions (lobe order <1) and the conventional regenerative effect (lobe order ≥ 1). While the stability boundary is independent of spindle speed (Fig. 2), the existing model can only be applied to the prediction of LFC in threading operations. The inability to model tool-workpiece engagement conditions [23] reasonably makes it unsuitable for predicting LFC in the milling process. The mode coupling effect has a significant impact on robotic milling's LFC due to the relatively weak rigid robot structure mode at low-frequency, so it is necessary to further consider the influence of the mode coupling effect without ignoring the modulated tool-workpiece engagement conditions.

According to a 2021 study by Celikag et al. [23], existing mode coupling chatter models applied to milling were based on threading operations and did not capture the characteristics of intermittent milling processes. Therefore, the authors established mode coupling and regenerative chatter prediction models based on existing stability research methods in robotic milling. The models were analyzed through milling experiments, which revealed the following findings: 1. The stability boundary obtained with the existing mode coupling chatter mechanism was inconsistent with the experimental results, and it ignored the modulated tool-workpiece engagement conditions of milling [24–26], showing spindle speed irrelevance and having obvious defects. 2. The stability boundary obtained with the existing regenerative chatter mechanism was inconsistent with the experimental results, but there was a certain velocity correlation in the low-speed region (0–500 rpm). This suggested that "mode coupling chatter does not exist." The study also noted that the assumption that the dynamic chip thickness depends only on the current vibration is not applicable to milling operations.

Similar validation experiments were conducted by the author's research team, which showed that the LFC stability boundary dominated by the robotic structure mode obtained by the existing mode coupling and regenerative chatter mechanisms was inconsistent with the experimental results. Therefore, using the regenerative effect at low spindle speed or the mode coupling effect at threading operation alone cannot describe the LFC of robotic milling.

To summarize, in the research of LFC of robotic milling, further investigation is necessary on modulated tool-workpiece engagement conditions, which have a tooth-passing frequency larger than the chatter frequency (lobe order <1), based on existing studies on the regenerative effect. This will enhance the applicability of the proposed model in higher spindle speed ranges. Subsequently, a modeling strategy that accounts for the mode coupling effect while considering modulated tool-workpiece engagement conditions should be developed.

In view of the problems this paper aims to address the issues in LFC research by undertaking the following research. Firstly, the cutting states involved in the development of LFC are analyzed, and the characteristics and identification methods of LFC states are summarized. Secondly, to overcome the assumption that process stability depends only on the current radial vibration, an LFC stability model is proposed to predict the stability of LFC, considering the modulated tool-workpiece engagement conditions. To address the challenge of accurately calculating the regenerative effect caused by LFC, a dynamic chip thickness calculation method based on surface renewal (SR) is introduced. Moreover, considering the mode coupling effect of robots, a dynamic modeling strategy based on impulse response function (IRF) is proposed. The paper combines the SR and IRF method to develop an LFC prediction method that considers both the modulated tool-workpiece engagement conditions and mode coupling effect. Finally, experimental verification is conducted, the sideband phenomenon observed in the chatter experiment is analyzed, and the paper is concluded and summarized.

This paper makes the following main contributions.

- Analyzing the problem of exponential growth in the LFC stability boundary predicted by the stability model based on the regenerative chatter mechanism when lobe order is less than 1, and proposing a surface renewal (SR) model that reasonably characterizes the modulated tool-workpiece engagement conditions. This model achieves an accurate calculation of dynamic chip thickness when lobe order is less than 1.
- Summarizing the reasons why stability models based on mode coupling chatter lack speed dependence and proposing a non-parametric dynamic characteristic characterization method based on the IRF method. This method effectively combines mode coupling effects with SR models to achieve the characterization of the speed dependence of LFC.
- Combining the IRF non-parametric dynamic characteristic characterization method with the SR model to propose an LFC stability prediction model. This model achieves LFC prediction across the entire spindle speed range.
- Verifying the accuracy of the proposed model through milling experiments with lobe orders both greater than and less than 1, and comparing it with the latest stability model of LFC.
- Explaining the sideband phenomenon in robotic milling based on the modulation principle, and verifying it through numerical simulation and experiment. This can be used as a signal to identify LFC when the lobe order is less than 1.

2. Low-frequency chatter (LFC) characteristics, influencing factors, existing research methods

2.1. Analysis of chatter characteristics in robotic milling

Studies on high-frequency and LFC in robotic milling reveal different mechanisms, allowing us to differentiate between the two types of chatter. High-frequency chatter occurs at frequencies close to the tool mode frequency, resulting in severe regenerative chatter and significant energy concentration [27] near the chatter frequency. This vibration signal is similar to the one shown in Fig. 3a, and is observed in both CNC machine milling and robotic milling [26,28]. LFC, on the other hand, is a common and important instability phenomenon in robotic milling, with a chatter frequency close to the frequency of the robotic structural mode, as shown in Fig. 3b at 13.75 Hz, which is consistent with previous literature [5,18]. Additionally, under the influence of modulation, sideband frequency modulation signals appear in the high-frequency part of the chatter spectrum, which is another characteristic of LFC. It should be noted that the sideband frequency phenomenon can be observed only in the high-speed region (lobe order <1).

Based on the above analysis, it is clear that LFC and high-frequency chatter have distinct differences. When using a tool with high stiffness, LFC dominates the processing stability of the system [3]. As the axial or radial cutting depth increases, LFC gradually appears, as shown in Fig. 4 which illustrates three typical states in the evolution process of LFC. Fig. 4a and d show the stable state, where an obvious forced vibration periodic signal can be observed in the vibration signal, and the displacement spectrum indicates almost no low-frequency vibration at this time. Fig. 4b and e show the steady-state vibration state, a transitional state before the occurrence of LFC. At this stage, an obvious low-frequency vibration periodic signal can be observed in the vibration signal, and signal modulation phenomena occur, with the low-frequency amplitude in the displacement spectrum at 18.19 μm. In this state, low-frequency vibration appears in the form of steady-state vibration, and the amplitude is typically in the range of several microns to tens of microns, with no apparent amplitude increase or instability. Previous research [29] has investigated the processing stability of robot milling under these conditions in depth. Fig. 4c and f show the chatter state, where low-frequency vibration increases significantly, and significant signal modulation phenomena occur. Low-frequency vibration plays a dominant role in the vibration signals, with the low-frequency amplitude in the displacement spectrum at 139.3 μm, much larger than the steady-state vibration shown in Fig. 4e. This state cannot continue processing as severe low-frequency vibration can cause serious damage to the robotic structure, tool, and workpiece. In this paper, the chatter state shown in Fig. 4c is studied, and the characteristics of LFC are summarized as follows.

1. The vibration spectrum is shown in Fig. 3b, and it is observed that the chatter frequency is close to the modal frequency of the robot structure.
2. The amplitude of low-frequency vibration signal in displacement spectrum is much larger compared to other frequencies, as shown in Fig. 4f.
3. The time-domain acceleration signal exhibits significant modulation phenomenon as shown in Fig. 4e, and the vibration spectrum consists of significant sideband frequency signal as shown in Fig. 3b.

The third characteristic of low-frequency vibration in robotic milling is a unique phenomenon. When low-frequency vibration occurs, a sideband signal with the frequency of this vibration as the interval appears around the tooth-passing frequency of the vibration spectrum. This signal is similar to the sideband signal used in gear and bearing fault diagnosis [30], and can serve as the symbol signal of LFC when the lobe order is less than 1. In Section 4, we carry out theoretical derivation and simulation analysis of the sideband signal to clarify its mechanism of appearance.

2.2. Analysis of influencing factors of LFC in robotic milling

The robotic type used in this study is the ABB IRB 6660. To analyze the influence factors of LFC in robotic milling systems, it is crucial to

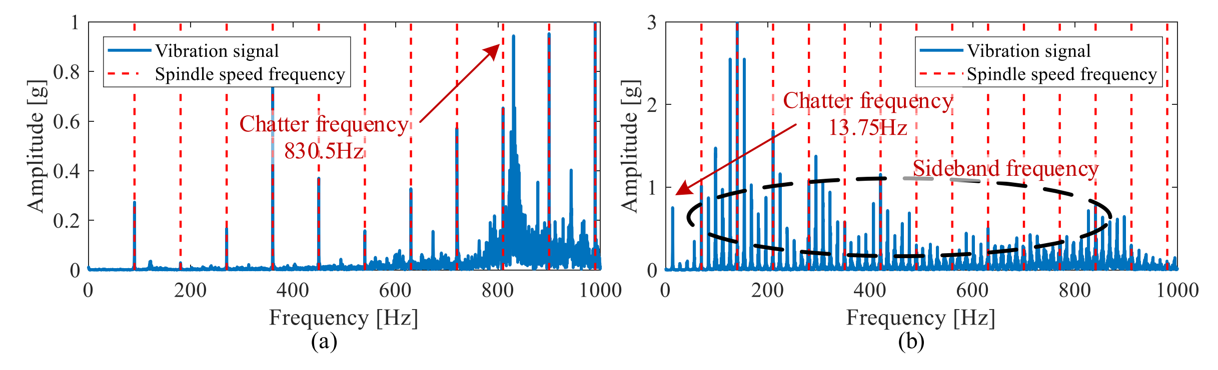


Fig. 3. Chatter in robotic milling: (a) High-frequency chatter (Low stiffness, long tool overhang, axial cutting depth is 0.6 mm, radial cutting depth is 6 mm, spindle speed is 5400 rpm), (b) Low-frequency chatter (High stiffness, short tool overhang, axial cutting depth is 1.2 mm, radial cutting depth is 12 mm, spindle speed is 4200 rpm). There is a significant difference between low-frequency chatter and high-frequency chatter in the vibration spectrum. The low-frequency chatter frequency is close to the natural frequency of the robot structure, and there are sideband frequencies in the whole bandwidth of the spectrum. The high-frequency chatter frequency is close to the tool natural frequency, and energy concentration often occurs near this frequency.

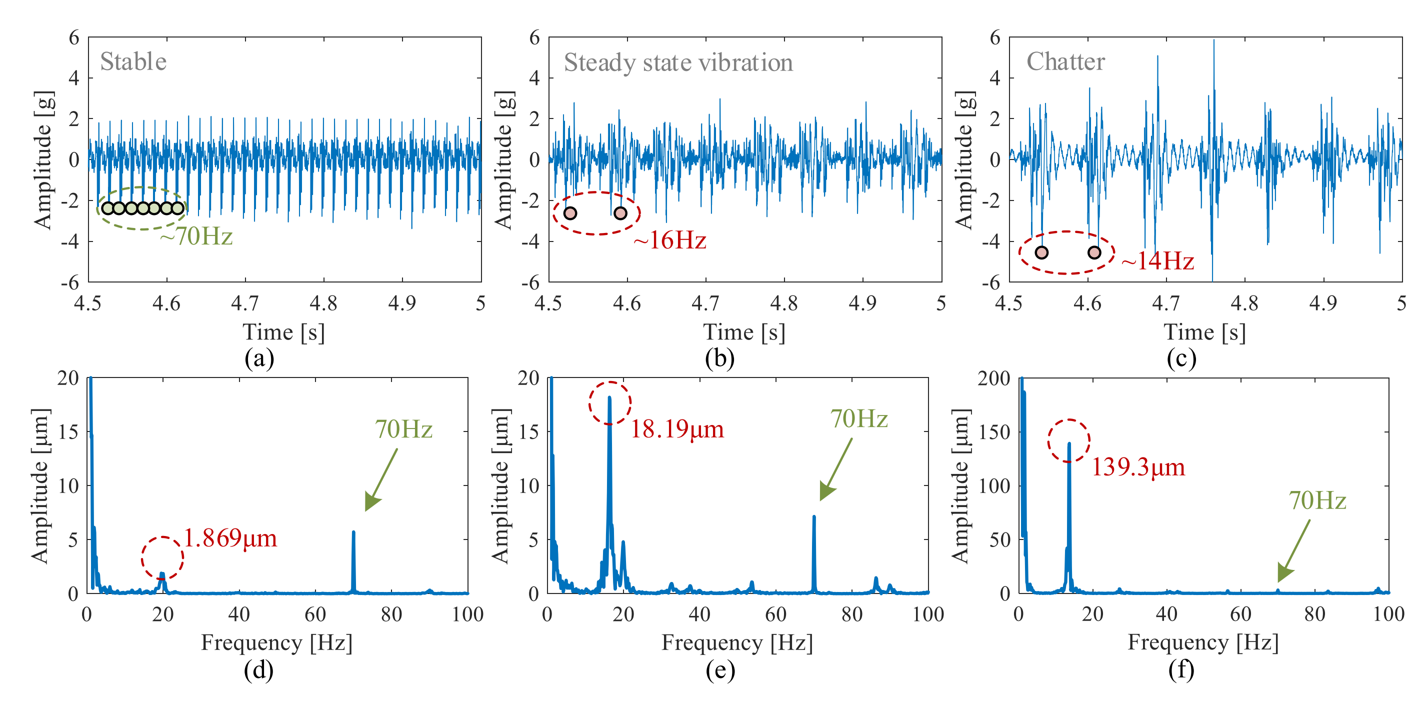


Fig. 4. Three typical states in the evolution process of low-frequency chatter: (a) and (d) Stable state, (b) and (e) Steady-state vibration state, (c) and (f) Chatter state. Significant modulation can be seen in the time domain signal of the chatter state.

identify the dynamic characteristics of the machining system and the engagement process of the cutting tool and workpiece during milling. To avoid the influence of high-frequency chatter dependent on tool modes in theoretical analysis and experimental verification, we used a bull-nosed tool (600-025A25-10H) with a diameter of 25 mm, and shortened the tool overhang length as far as possible to maximize tool rigidity. The IBAG high-power spindle (HT 170.12AI 22 CHKPV) was selected to adapt to milling with large axial cutting depth. The parameters of robotic milling system are shown in Table 1.

The possibility of chatter in a machining system is closely related to its dynamic characteristics. This is why the chatter frequency often coincides with the modal frequency. In this study, we aim to uncover the cause of LFC in robotic milling systems. To achieve this, it is necessary to test and analyze the dynamic characteristics of the robotic milling system. The dynamic characteristics of the system consist of two parts: the low-frequency part (robot) and the high-frequency part (tool). Due to the significant difference in frequency between the two parts, it is difficult to measure them simultaneously using traditional accelerometers. Therefore, to obtain the frequency response distribution of the robotic milling system across its complete bandwidth, we used a 3D scanning laser Doppler vibrometer to conduct modal tests. The test setup is illustrated in Fig. 5, and the test results are presented in Fig. 6.

Table 1
Robotic milling system parameters for illustration.

Item	Value
Robot weight (kg)	1730
Robot handing capacity (kg)	205
Robot reach (m)	1.93
Spindle constant torque (Nm)	31.8
Spindle constant output (kW)	30
Spindle Min. Rpm	0
Spindle Max. Rpm	12,000
Tool diameter (mm)	25
Tool teeth number	3
Tool helix angle (deg)	7
Tool overhang length (mm)	60

The analysis of the dynamic flexibility of different modes is essential

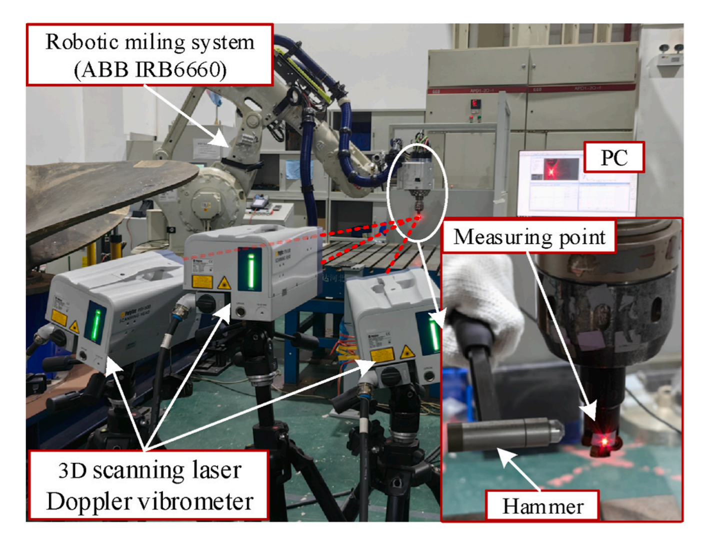


Fig. 5. Modal test setup and robotic milling system. In the experiment, a 3D scanning laser Doppler vibrometer is used so that the modes of the tool and the robot can be measured simultaneously.

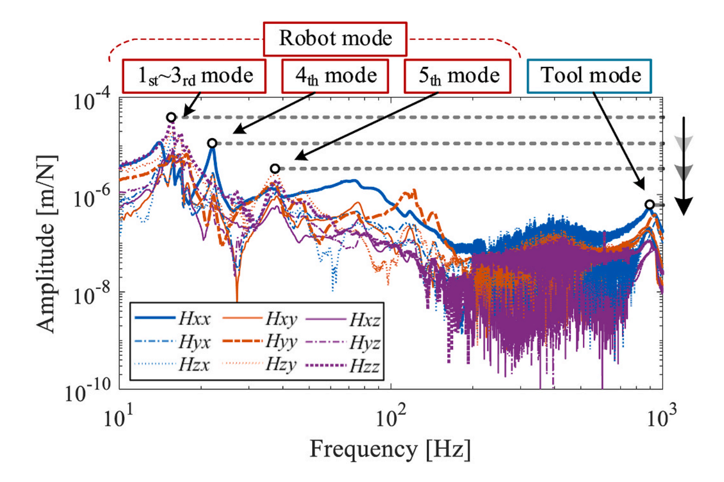


Fig. 6. Modal characteristics of robotic milling system. The robot mode is concentrated within 50Hz, and the dynamic flexibility is much smaller than the tool mode. Robotic joint configuration (Joint 1–6): 18.83°, 35.14°, 42.10°, 26.96°, −45.37°, 160.35°.

to locate the weak rigid parts of the robotic milling system. When using a large size, short overhang length tool for milling operations, low-frequency modes (dominated by the robotic structure) are significantly less rigid than high-frequency modes (dominated by the tool). This lack of dynamic stiffness in the low-frequency modes leads to low-frequency vibration with large amplitude, resulting in complex dynamic chip thickness changes. As a result, it is impossible to obtain an accurate stability boundary by analyzing only the high-frequency chatter dominated by the tool structure, unlike in CNC machine tool processing systems. The weakness of the robotic milling system lies in the robot structure itself, and LFC is the key problem that limits its efficiency improvement. In addition to locating the weak rigid parts of the system, it is crucial to compare the modal complexity of the low-frequency and high-frequency modes. It is observed that the low-frequency mode has many modes with closely spaced natural frequencies, making the mode coupling phenomenon more likely to occur [31]. Therefore, when analyzing the robotic milling stability with complex modal characteristics, the mode coupling effect in the low-frequency modes of the robot must be fully considered. The strategy of using a single mode for stability analysis is no longer applicable, and a more comprehensive approach that considers all modal interactions is necessary.

After analyzing the dynamic characteristics of the robotic milling system, we have identified two critical points. Firstly, LFC significantly limits the efficiency improvement of the robotic milling system. Secondly, the stability analysis of LFC in the robotic milling system cannot be conducted using a single modal modeling strategy, and the impact of mode coupling must be taken into consideration.

In addition to the machining system's dynamic characteristics, the machining method significantly affects the occurrence of chatter. Different machining methods result in different tool-workpiece engagement processes, leading to different dynamic cutting force manifestations. As illustrated in Fig. 7, the threading operation differs significantly from the milling operation. In threading, the tool cuts a new surface continually; its instantaneous chip thickness is determined solely by the current cutting's tool path $X(t)$, and only the vibration effect on the current tool path needs to be considered. The instantaneous chip thickness can be expressed as follows:

$$h_b(t) = h_{b0}(t) + \underbrace{\delta h_b(t)}_{T_c-periodic}, \tag{1}$$

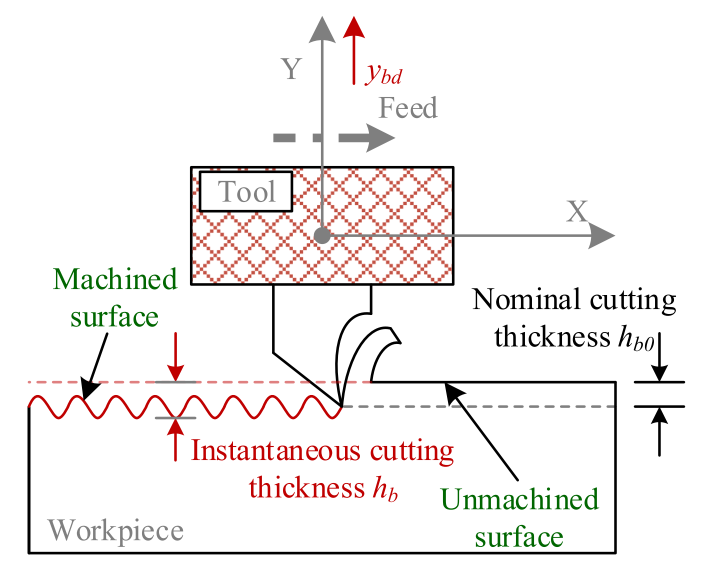


Fig. 7. The tool-workpiece engagement process of threading operation. There is no need to consider time delay in dynamic chip thickness calculation.

where.

- $h_{b0}(t)$ is the nominal chip thickness;
- $\delta h_b\ (t) = y_{bd}\ (t)$ is the current vibration in the Y direction of T_c-periodic. $T_c = 1/f_c$, where f_c indicates the chatter frequency.

However, for milling, the instantaneous chip thickness is dependent on not only the current vibration but also the vibration marks left by the previous tooth on the workpiece surface, referred to as the regenerative effect [24]. Consequently, the instantaneous chip thickness should be calculated by both the current cutting tooth path $X(t)$ and the effective cutting tooth path $X\ (t\text{-}\tau_0)$. When considering ideal cutting tool with the regular, constant pitch and negligible run-out, delay time τ_0 is the tooth passing period, and in more general cases, the delay time should be the spindle revolution period or longer, detailed reference [32,33], this paper will not conduct in-depth study on this aspect. Considering the effect of vibration on the tool path, the instantaneous chip thickness $h_m(t)$ can be expressed as:

$$h_m(t) = \underbrace{h_{m0}(t)}_{\tau_0-periodic} + \underbrace{\delta h_m(t)}_{T_c-periodic}, \tag{2}$$

where.

- $h_{m0}(t)$ is the nominal chip thickness with τ_0-periodicity;
- $\delta h_m(t) = \cos(\varphi_{ij}(t))(x_{md}(t) - x_{md}(t-\tau_0)) - \sin(\varphi_{ij}(t))(y_{md}(t) - y_{md}(t-\tau_0))$ is the regenerative vibration of T_c-periodic. $T_c = 1/f_c$, f_c indicates the chatter frequency. $x_{md}(t)$ and $y_{md}(t)$ are the current vibrations in the X and Y directions, $x_{md}\ (t\text{-}\tau_0)$ and $y_{md}\ (t\text{-}\tau_0)$ are the vibrations of the previous time τ_0 in the X and Y directions.

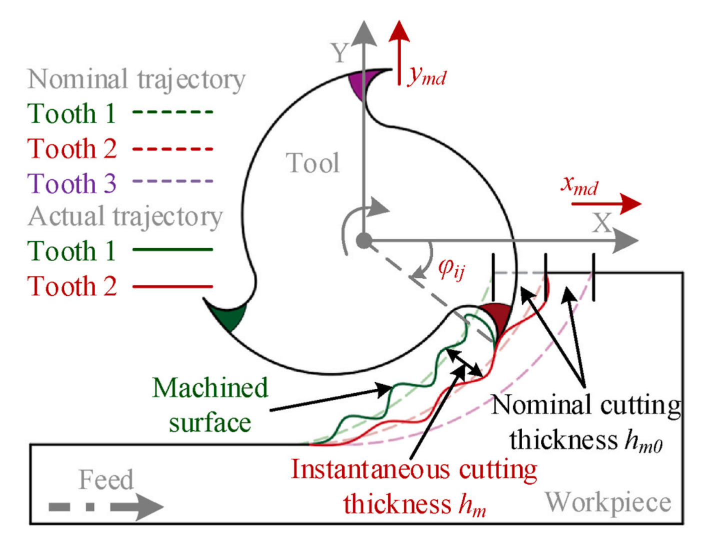


Fig. 8. The tool-workpiece engagement process of milling operation. There is need to consider time delay in dynamic chip thickness calculation. When low-frequency chatter occurs, complex modulated tool-workpiece engagement conditions may occur.

Table 2
Influencing factors and coping strategies of robotic low-frequency chatter.

Type	Features	Effect	Strategy
Robotic dynamic characteristics	Complex mode characteristics	A single mode cannot reflect the true stability result	Consideration of mode coupling effect by IRF method
	Mode coupling effect	Obvious force-position feedback between the modes	
Tool-workpiece engagement conditions	High vibration amplitude	Tool-workpiece separation	A surface renewal model was established to achieve accurate calculation of dynamic chip thickness
	Low chatter frequency	Dynamic chip thickness has a large period	

In the case of common high-frequency chatter, lobe order is typically ≥1 and $\tau_0 \geq T_c$, causing h_{mij}(t) to be approximately τ_0-periodic. However, LFC modulates the tool-workpiece engagement conditions in such a way that they become periodic within multiple spindle revolutions, rather than a single revolution (lobe order <1). Consequently, the period of the instantaneous chip thickness is also extended. Furthermore, larger vibrations can cause the tool-workpiece separation, resulting in a non-constant delay time τ_0, leading to symmetric breaking [32,33]. The analysis and modeling of this phenomenon is essential to understand and predict LFC. Thus, the original stability calculation method that only considers the instantaneous chip thickness change within one tooth-passing period is no longer appropriate. The period of regenerative vibration in Eq. (2) should be equal to or greater than one chatter period, which is longer than the tooth-passing period.

Through the analysis of the machining method used in robotic milling, two key points were identified: (1) The modulated tool-workpiece engagement conditions are inherent in robotic milling, and their influence must be considered in stability analysis. (2) The extremely low chatter frequency of LFC changes the basic properties of dynamic chip thickness. As a result, the stability calculation method that only considers instantaneous chip thickness changes within one or a few tooth-passing periods is no longer applicable.

Based on the analysis of the dynamic characteristics and machining methods of robotic milling, several critical factors affecting LFC and the strategies proposed in this paper can be summarized in Table 2.

2.3. Analysis and comparison of existing LFC prediction methods

The LFC in robotic milling has been a popular topic in stability research. Various studies have explained and predicted LFC from different angles. Regenerative chatter theory has been used in some research to develop stability models of LFC [6,8]. However, the modulated tool-workpiece engagement conditions caused by extremely low chatter frequency are often ignored in the analysis process, which means that stability prediction can only be achieved in the low-speed region (≤2000 rpm, lobe order ≥1 [6,8,13]). In the medium-high speed region (>2000 rpm, lobe order <1), the predicted stability boundary typically shows an unreasonable increase as spindle speed increases.

Other research has relied on mode coupling theory to establish stability models of LFC [3,17,18], which capture the mode coupling effect

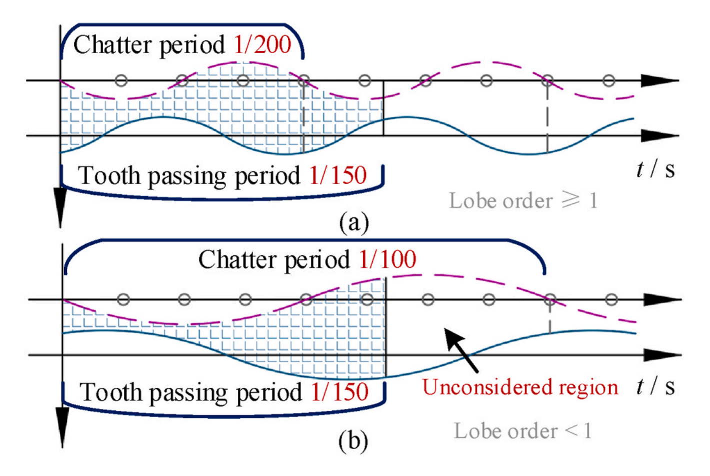


Fig. 9. The effect of chatter frequency on stability calculation, (a): Chatter frequency is higher than the tooth passing frequency (Lobe order ≥1), (b): Chatter frequency is lower than the tooth passing frequency (Lobe order <1).

that exists in the dynamic characteristics of the robot. However, the tool-workpiece engagement conditions in robotic milling are often not properly modeled, resulting in the loss of spindle speed dependence of the stability boundary. Both types of models have their own unique characteristics, which explain some aspects of the mechanism of LFC to a certain extent. To better understand the causes of LFC, this section will analyze the strengths and weaknesses of existing models in combination with the discussion of factors affecting LFC in section 2.2. By doing so, key issues in predicting LFC in robot milling can be extracted.

Most stability models of LFC based on regenerative chatter theory rely on two assumptions

1. The stability of the entire cutting process can be characterized by the calculation result of one tooth-passing period.
2. The tooth passing period T_{tp} ($T_{tp} = 60/Nn$, where N is the number of teeth, n is the spindle speed) is taken as the delay time τ_0.

In most cases, these assumptions are reasonable and can better characterize the tool-workpiece engagement conditions. However, there are at least two cases where a model based on both of these assumptions is no longer applicable. The first case occurs when the chatter frequency is lower than the tooth-passing frequency, resulting in a lobe order of less than one. The second case is when there is vibration with too large an amplitude during processing, such as during the critical state of LFC or steady-state vibration with a large amplitude.

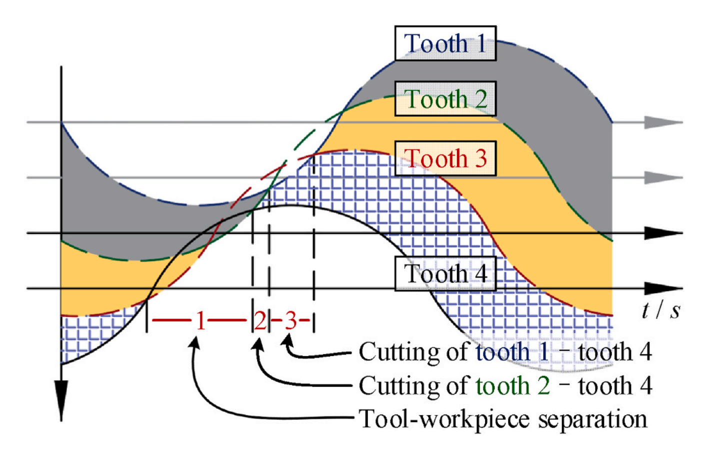


Fig. 10. The effect of chatter amplitude on the size of instantaneous chip thickness in stability calculations. Large probability will cause the tool-workpiece separation and other states, resulting in the nonlinear tool work-piece engagement conditions.

In the first case, the traditional stability model ensures that the lobe order is greater than or equal to one (with the chatter frequency f_c higher than the tooth-passing frequency f_{tp}). Otherwise, the instantaneous chip thickness variation within a single tooth-passing period T_{tp} will not fully capture all the variation caused by the chatter. Fig. 9 illustrates this issue with diagrams of instantaneous chip thickness, using a tooth-passing frequency of 150 Hz and chatter frequencies of 200 Hz and 100 Hz (approximately equal to the natural frequency), respectively. When the chatter frequency is higher than the tooth-passing frequency, as shown in Fig. 9a, the lobe order is greater than or equal to one, and the tooth-passing period fully captures the variation of instantaneous chip thickness due to chatter. Thus, this method can accurately describe the change in stability. However, when the chatter frequency is lower than the tooth-passing frequency, as shown in Fig. 9b, the lobe order is less than one, and only part of the chatter-induced variation in instantaneous chip thickness is considered. As a result, this method cannot accurately describe the change in stability. Therefore, in the study of LFC in robotic milling, it is essential to consider the problem of low chatter frequency (10–30 Hz) in the medium-high speed range (>2000 rpm, with lobe order less than one), in order to accurately capture the dynamic changes in chip thickness during the entire chatter period, and to describe the modulated tool-workpiece engagement conditions.

In the second case, the traditional stability model calculates the dynamic part of the instantaneous chip thickness by $d(t)$-d (t-T_{tp}), assuming that the tooth-passing period T_{tp} is the time delay. However, this method is only applicable when the chatter amplitude is lower than the feed per tooth, and there is no tool-workpiece separation in the cutting process. In the case of LFC in robotics with large amplitude and frequent tool-workpiece separation, it is difficult to consider the change in instantaneous chip thickness caused by tool-workpiece separation when using this method. Furthermore, continuous tool-workpiece separation can change the time delay and complicate the calculation of instantaneous chip thickness. Fig. 10 shows that in milling, when the amplitude of chatter vibration is large, tool-workpiece separation

Table 3
Characteristics and application fields of existing methods.

	Threading operation	Milling with lobe order ≥1	Milling with lobe order <1	Features
Regenerative chatter model [6]	✓	✓	×	It can be used to predict the stability of LFC when lobe order ≥1. However, the prediction accuracy cannot be guaranteed because the mode coupling effect is not considered. It is not suitable for the characterization of modulated tool-workpiece engagement conditions of LFC, cannot fully consider the change of instantaneous chip thickness, and is not suitable for the prediction of LFC when lobe order <1.
Mode coupling chatter model [3]	✓	×	×	Without accurate characterization of tool-workpiece engagement conditions in milling, it is not suitable for milling stability prediction.

occurs, resulting in zero instantaneous chip thickness in region 1. In addition, if there is tool-workpiece separation during the cutting process, the instantaneous chip thickness is formed by the vibration trajectory of the nearest tooth without tool-workpiece separation and the vibration trajectory of the current tooth, as seen in region 2. For example, if tool-workpiece separation occurs for tooth 3, the current instantaneous chip thickness is formed by the vibration trajectory of tooth 2 and tooth 4. Similarly, in region 3, when both tooth 2 and tooth 3 have tool-workpiece separation, the current instantaneous chip thickness is formed by the vibration trajectory of tooth 1 and tooth 4. These phenomena change the tool-workpiece engagement conditions and need to be considered in the research of LFC in robotic milling. Therefore, accurately describing the dynamic chip thickness requires consideration of the problem of large chatter amplitude.

The use of the two assumptions mentioned above for LFC stability prediction can result in unreasonable increases in the stability boundary at medium-high spindle speeds, as demonstrated in Fig. 1. Scholars have attempted to address the problem of LFC by focusing on the mode coupling effect present in the robot's dynamic characteristics, as seen in Refs. [3,17,18]. However, these models do not accurately account for the tool-workpiece engagement conditions in milling, rendering them unsuitable for milling applications. In a recent study [23], the limitations of these models were thoroughly analyzed, and it was found that the mode coupling chatter model cannot be applied to milling due to the false assumption that the dynamic chip thickness depends solely on the current normal vibration on the chip surface. The article explains, “This is mainly due to the false assumption which states that the dynamic chip thickness depends only on the current normal vibration on the chip surface in milling” [23]. Consequently, such models are more appropriate for threading operations, as shown in Fig. 7.

Table 3 summarizes the characteristics and application fields of existing methods for predicting robotic LFC. However, as shown in Tables 2 and 3, there is a common problem with these models: they do not accurately characterize the tool-workpiece engagement conditions, leading to large errors in dynamic chip thickness and ultimately failing to predict stability boundaries. Moreover, the complex mode characteristics of robotic milling systems require models that can consider mode coupling effects. To address the issue of inaccurate characterization of tool-workpiece engagement conditions, this paper proposes an SR model based on geometry, which accurately calculates dynamic chip thickness. Additionally, we use IRFs to replace dynamic parameters in traditional modeling and establish a stability model that considers mode coupling effects based on IRFs.

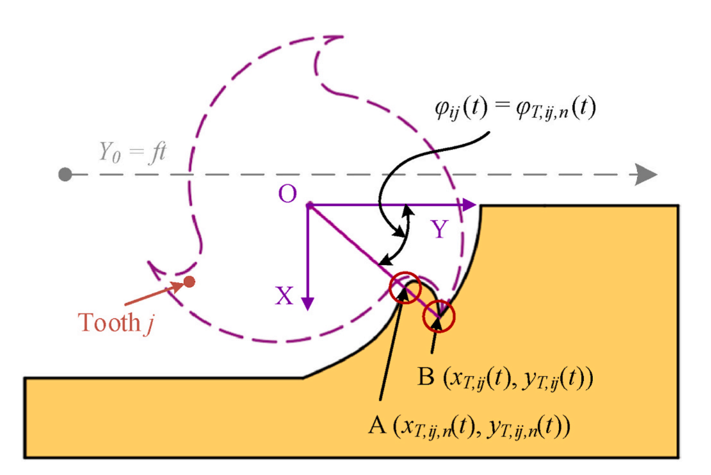


Fig. 11. Surface update geometry model. Point A is the cutting point, point B is the blade point, and the instantaneous chip thickness is the workpiece thickness between point A and point B.

3. LFC stability model for robotic milling considering mode coupling effect and modulated tool-workpiece engagement conditions

In this section, we present an LFC stability model that accounts for modulated tool-workpiece engagement conditions and the complex mode coupling of robotic milling systems. Our approach builds on the analysis presented in Sections 2.2 and 2.3. Firstly, we introduce a surface renewal (SR) model that considers the regenerative effect from a geometric perspective. By incorporating the modulated tool-workpiece engagement conditions into the cutting force modeling, the SR model enables us to calculate the dynamic chip thickness more accurately. Secondly, we establish an LFC stability model that accounts for both the modulated tool-workpiece engagement conditions and the mode coupling effect using the impulse response function (IRF) method. This model is compared to the existing stability model for explaining LFC.

3.1. Surface renewal (SR) model

The geometric model of the surface update is shown in Fig. 11. In the tool coordinate system (XOY), the blade coordinate B at any time can be expressed as:

$$\begin{cases} x_{T,ij}(t) = R\sin(\varphi_{ij}(t)) + x_{lev,ij}(t) \\ y_{T,ij}(t) = R\cos(\varphi_{ij}(t)) + y_{lev,ij}(t) \end{cases}, \tag{3}$$

where R represents tool radius, t represents time, $x_{lev,ij}(t), y_{lev,ij}(t)$ represents the additional vibration displacement caused by LFC, $\varphi_{ij}(t)$ denotes immersion angle, i and j represent the number of cutting elements and teeth number of the tool, respectively. During the cutting, the coordinates $(x_{T,ij}(t_n), y_{T,ij}(t_n))$ and time t_n of the blade point in the tool coordinate system are recorded. The blade point will be converted to the cutting point. As the cutting point is located on the workpiece, the coordinates of the cutting point in the tool coordinate system change with the cutting progress, which can be expressed as:

$$\begin{cases} x_{T,ij,n}(t) = x_{T,ij}(t_n) - \left[x_{lev,ij}(t) - x_{lev,ij}(t_n)\right] \\ y_{T,ij,n}(t) = Y_{T,ij}(t_n) - \left[y_{lev,ij}(t) - y_{lev,ij}(t_n)\right] - (t - t_n)f \end{cases}, \tag{4}$$

where f represents the feed speed. It follows that the angle $\varphi_{T,ij,n}(t)$ of the cutting point in the tool coordinate system also changes with the cutting process and can be expressed as:

$$\varphi_{T,ij,n}(t) = \arctan\left(\frac{x_{T,ij,n}(t)}{y_{T,ij,n}(t)}\right). \tag{5}$$

Thus, the coordinates A $(x_{T,ij,n}(t), y_{T,ij,n}(t))$ and the angle $\varphi_{T,ij,n}(t)$ of all cutting points on the workpiece surface in the tool coordinate system are obtained.

As shown in Fig. 12, point B_n = B (t_n) $(x_{T,ij}(t_n), y_{T,ij}(t_n))$ is the coordinate of the blade present in the tool coordinate system at the current moment. $\varphi_{ij}(t_n)$ is the immersion angle at the current moment, and $n = 2$ or 3 in the figure. For simplicity, the cutting point corresponding to the angle $\varphi_{T,ij,n}(t)$ when $\varphi_{T,ij,n}(t) = \varphi_{ij}(t)$ is referred to as the cutting interference point at this moment in the following. This implies that the cutting interference point is the cutting point on the same line as the blade point and the tool center point.

Fig. 12 illustrates the cutting process for a rotating blade with multiple teeth. In Fig. 12a, the blade point B_2 is positioned between the cutting interference point A_2 and the tool center point O_2. At this point, no cutting occurs and the current values of the instantaneous chip thickness $(h_{ij}(t_2))$ and cutting force are zero. When the tool rotates by one tooth, as shown in Fig. 12b, the cutting interference point A_3 remains the same as in Fig. 12a because the previous tooth did not cut the current workpiece surface. However, the cutting interference point A_3 is now located between the blade point B_3 and the tool center point O_3,

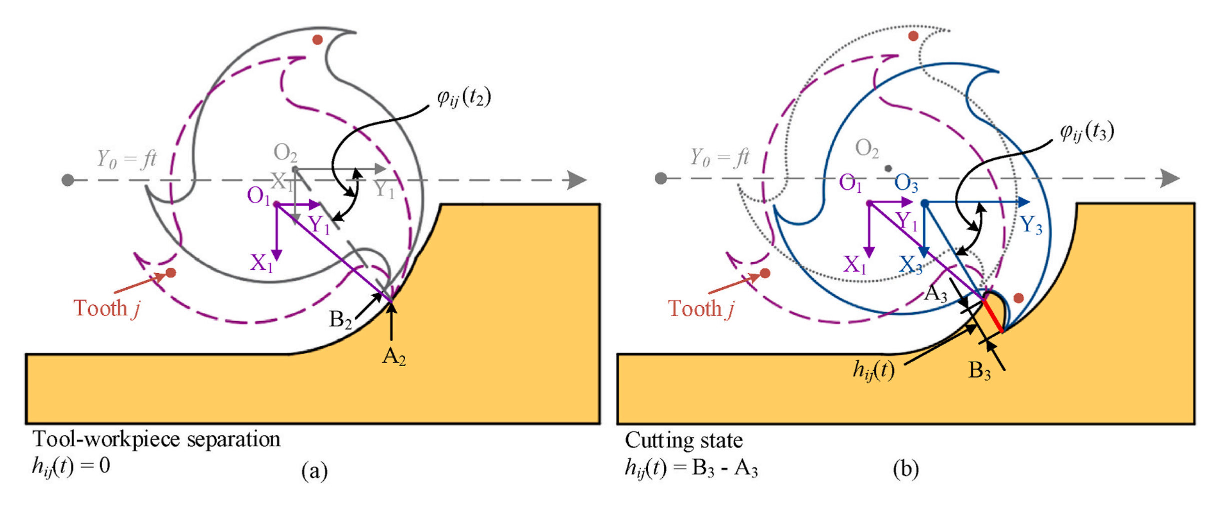


Fig. 12. Instantaneous chip thickness calculation model considering SR. (a) Tool-workpiece separation, (b) Calculation method of dynamic chip thickness after tool-workpiece separation.

resulting in cutting. The instantaneous chip thickness ($h_{ij}(t_3)$) is determined by the distance between the cutting interference point A_3 and the blade point B_3. The following function can be used to make this determination:

$$\begin{cases} g_{ij}(t) = 1, \text{if}\left(\sqrt{(x_{T,ij,n}(t))^2 + (y_{T,ij,n}(t))^2} < \sqrt{(x_{T,ij}(t))^2 + (y_{T,ij}(t))^2}, \text{when}\left(\varphi_{T,ij,n}(t) = \varphi_{ij}(t)\right)\right) \\ g_{ij}(t) = 0, \text{if}\left(\sqrt{(x_{T,ij,n}(t))^2 + (y_{T,ij,n}(t))^2} \geq \sqrt{(x_{T,ij}(t))^2 + (y_{T,ij}(t))^2}, \text{when}\left(\varphi_{T,ij,n}(t) = \varphi_{ij}(t)\right)\right) \end{cases}, \tag{6}$$

where $g_{ij}(t)$ denotes the unit step function to judge whether cutting occurs, $g_{ij}(t) = 1$ means cutting occurs, and $g_{ij}(t) = 0$ means cutting does not occur. On the other hand, the workpiece surface needs to be updated

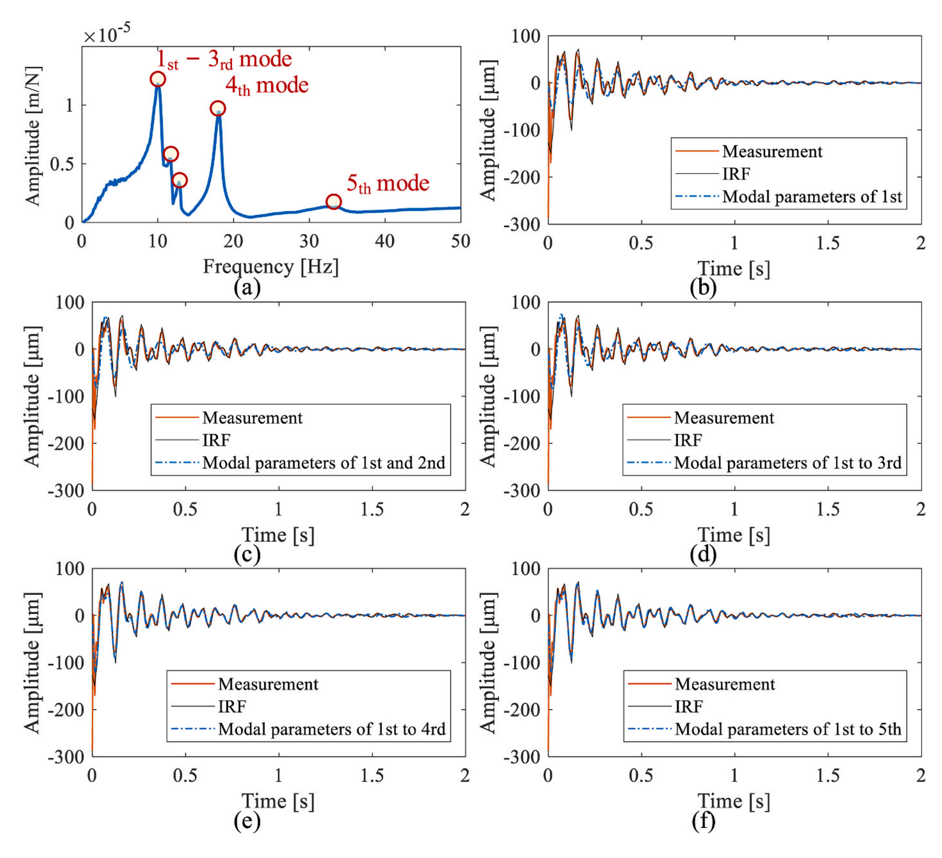


Fig. 13. IRF signal verification in a certain posture (Joint 1–6: 23.65°, 6.36°, 50.74°, 29.48°, −54.57°, 161.86°.) and a certain direction (X direction). (a) Frequency response function, (b) Only the first mode is considered, (c) Consider modes of 1_{st} and 2_{nd}, (d) Consider modes of 1_{st} to 3_{rd}, (e) Consider modes of 1_{st} to 4_{th}, (f) Consider modes of 1_{st} and 5_{th}.

during the cutting, as shown in Eq. (4), by replacing the cutting interference point A_3 with the current blade point B_3 as the new cutting interference point for subsequent calculations.

When cutting occurs, the expression of instantaneous chip thickness is as follows:

$$h_{ij}(t) = \left(x_{T,ij}(t) - x_{T,ij,n}(t)\right)\sin\varphi_{ij}(t) + \left(y_{T,ij}(t) - y_{T,ij,n}(t)\right)\cos\varphi_{ij}(t). \tag{7}$$

Combining Eq. (6) with Eq. (7), the instantaneous cutting force model considering SR is shown below:

we conducted an impact test on a certain direction of the robot and obtained multi-order modal parameters. We drew the response signal under unit pulse excitation by considering the modes in different bandwidths. By comparing this signal with the IRF signal obtained by the proposed method, we found that the IRF retains more modal information and improves the accuracy of the model. The IRF signal obtained by selecting the bandwidth of 0–50 Hz is basically consistent with the standard signal, which can effectively preserve the multi-mode characteristics of the robot while improving computational efficiency. Fig. 13 shows the comparison of the response signal and the IRF signal.

$$\begin{cases} F_x(t) = \sum_{i=1}^{N}\sum_{j=1}^{M} g_{ij}(t)h_{ij}(t)\left(-k_{tc}\cos(\varphi_{ij}) - k_{rc}\sin(\varphi_{ij})\sin(\alpha_{ij}) - k_{ac}\sin(\varphi_{ij})\cos(\alpha_{ij})\right)dz/\sin(\alpha_{ij}) \\ F_y(t) = \sum_{i=1}^{N}\sum_{j=1}^{M} g_{ij}(t)h_{ij}(t)\left(k_{tc}\sin(\varphi_{ij}) - k_{rc}\cos(\varphi_{ij})\sin(\alpha_{ij}) - k_{ac}\cos(\varphi_{ij})\cos(\alpha_{ij})\right)dz/\sin(\alpha_{ij}) \\ F_z(t) = \sum_{i=1}^{N}\sum_{j=1}^{M} g_{ij}(t)h_{ij}(t)\left(k_{rc}\cos(\alpha_{ij}) - k_{ac}\sin(\alpha_{ij})\right)dz/\sin(\alpha_{ij}) \end{cases}, \tag{8}$$

where $x_{T,ij,n}(t), y_{T,ij,n}(t)$ is the coordinate of the cutting interference point on the workpiece surface in the tool coordinate system at time t, and $x_{T,ij}(t), y_{T,ij}(t)$ is the coordinate of the blade in the cutting state at time t in the tool coordinate system. K_{tc}, k_{rc}, k_{ac} are the cutting force coefficient, α_{ij} is the axial contact angle.

3.2. LFC stability model based on IRF method

To consider the regenerative effect, we replace the traditional time-delay model with the surface renewal model, which avoids the calculation error of instantaneous chip thickness caused by the separation phenomenon of multi-tooth. This enables us to incorporate the modulated tool-workpiece engagement conditions into the stability prediction of LFC. To account for the mode coupling effect, we use IRF with a certain bandwidth to characterize the modal characteristics of each direction. The IRF can retain more modal information compared to multi-modal parameters and is more suitable for the SR model established from the geometric level. Compared to the multi-modal parameters, the non-parametric characterization of system dynamic characteristics based on IRF retains more modal information while significantly reducing the computation required.

To validate our approach, we conducted an impact test and used a 3D scanning laser Doppler vibrometer to test the response signal, as shown in Fig. 5. We selected a bandwidth of 0–50 Hz, which we verified as suitable in Fig. 13, and performed band-pass filtering on the response signal. We calculated the impulse using the force signal feedback from the hammer and divided the obtained response signal by the impulse to obtain the IRF signal.

The aim of this study is to establish a stability model of LFC that considers modulated tool-workpiece engagement conditions and the robotic complex mode coupling. In this section, we present the process of verifying the filter bandwidth range and obtaining the impulse response functions in all directions. To verify the filter bandwidth range,

Finally, Fig. 14 displays the impulse response functions in all directions.

Fig. 15 illustrates the impact of dynamic characteristics and the mode coupling on the vibration response of a robot in three degrees of freedom (DOFs). Specifically, the forces in each direction can influence the robot's vibration response in any direction. Mathematically, this relationship can be expressed as follows:

$$\begin{bmatrix} X(\omega) \\ Y(\omega) \\ Z(\omega) \end{bmatrix} = \begin{bmatrix} \mathbf{H}_{xx} & \mathbf{H}_{xy} & \mathbf{H}_{xz} \\ \mathbf{H}_{yx} & \mathbf{H}_{yy} & \mathbf{H}_{yz} \\ \mathbf{H}_{zx} & \mathbf{H}_{zy} & \mathbf{H}_{zz} \end{bmatrix} \begin{bmatrix} \mathbf{F}_x(\omega) \\ \mathbf{F}_y(\omega) \\ \mathbf{F}_z(\omega) \end{bmatrix}, \tag{9}$$

where $X(\omega)$, $Y(\omega)$, $Z(\omega)$ represent the vibration of the robot end in the X, Y, and Z directions respectively, $\mathbf{H}_{ij}$ represents the FRFs of the robot end in the i direction responding to the excitation in the j direction, $\mathbf{F}_i(\omega)$ represents the cutting force on the robot end in i direction. The expression is as follows:

$$\begin{cases} \mathbf{H}_{ij} = [H_{1,ij} \quad H_{2,ij} \quad \cdots \quad H_{m,ij}]_{(1\times m)} \\ \mathbf{F}_i = [F_i \quad F_i \quad \cdots \quad F_i]^{\mathrm{T}}_{(m\times 1)} \end{cases}, (i,j = x,y,z). \tag{10}$$

In Fig. 15, m represents the modal order. Taking the X direction as an example. Converting Eq. (9) to the time domain gives the following expression:

$$\begin{matrix} M_{1,xx}\ddot{X}_{x1}(t) + C_{1,xx}\dot{X}_{x1}(t) + K_{1,xx}X_{x1}(t) + \cdots + M_{m,xx}\ddot{X}_{xm}(t) + C_{m,xx}\dot{X}_{xm}(t) + K_{m,xx}X_{xm}(t) = F_x(t) \\ M_{1,xy}\ddot{X}_{y1}(t) + C_{1,xy}\dot{X}_{y1}(t) + K_{1,xy}X_{y1}(t) + \cdots + M_{m,xy}\ddot{X}_{ym}(t) + C_{m,xy}\dot{X}_{y2}(t) + K_{m,xy}X_{ym}(t) = F_y(t) \\ M_{1,xz}\ddot{X}_{z1}(t) + C_{1,xz}\dot{X}_{z1}(t) + K_{1,xz}X_{z1}(t) + \cdots + M_{m,xz}\ddot{X}_{zm}(t) + C_{m,xz}\dot{X}_{z2}(t) + K_{m,xz}X_{zm}(t) = F_z(t) \end{matrix}, \tag{11}$$

where $M_{n,ij}$, $C_{n,ij}$, $K_{n,ij}$ are the modal parameters of each order in each direction, and X_{xn}, X_{yn}, X_{zn} represent the vibration displacement response of each mode in the x-direction caused by the cutting forces in the x, y, and z directions. The expression is as follows:

$$X(t) = X_{x1}(t) + X_{y1}(t) + X_{z1}(t) + \cdots + X_{xm}(t) + X_{ym}(t) + X_{zm}(t). \tag{12}$$

In this paper, the IRF method [34] is used for the time-domain solution of the vibration signal. Using IRF instead of modal parameters, Eq. (11) and Eq. (12) can be rewritten as follows:

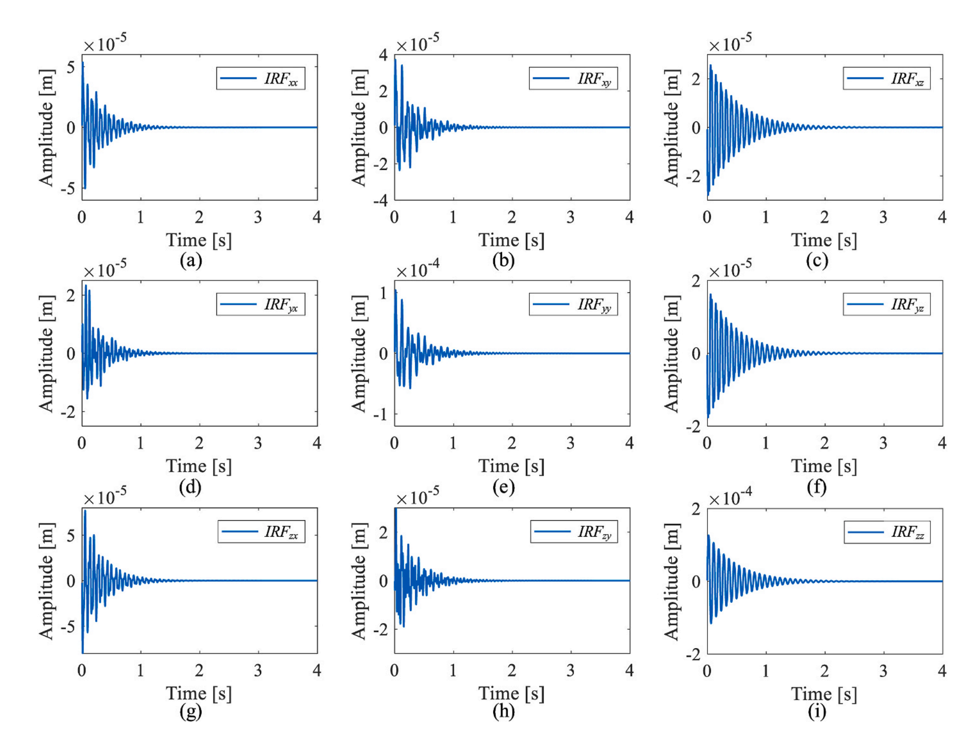


Fig. 14. Impulse response functions in all directions. (a) IRF_{xx}, (b) IRF_{xy}, (c) IRF_{xz}, (d) IRF_{yx}, (e) IRF_{yy}, (f) IRF_{yz}, (g) IRF_{zx}, (h) IRF_{zy}, (i) IRF_{zz}.

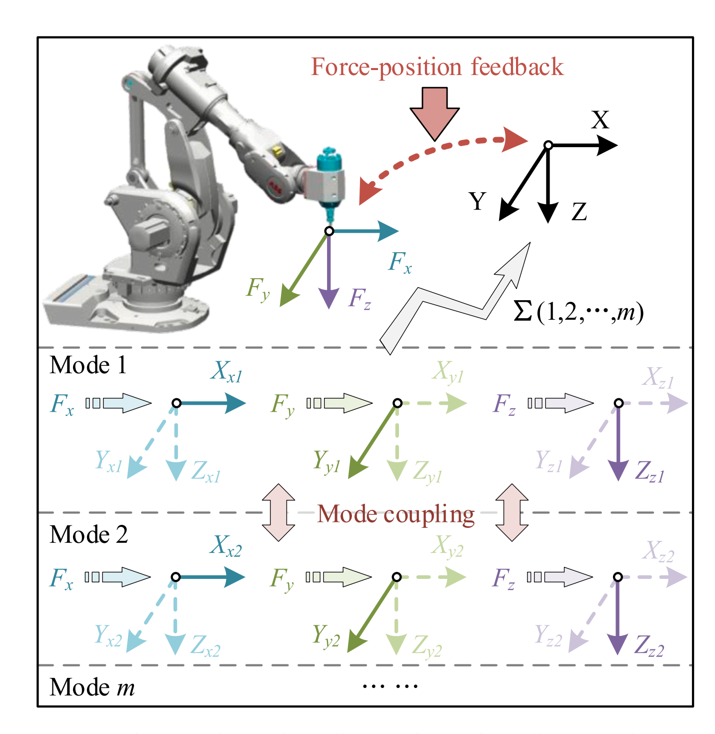


Fig. 15. Robotic mode coupling effect. Mode coupling effects exist between modes with closely spaced natural frequencies but different modal properties and directions at multiple degrees of freedom. When a mode is excited in milling process, the vibration feedback between the various degrees of freedom will excite the adjacent modes, and the vibration of the adjacent modes will cause new dynamic cutting forces. The force-position feedback exists between the modes, which leads to the sharp increase of the vibration of a mode to form self-excited vibration.

$$X(k\tau+\tau)=\sum_{n=1}^{k}\left(F_x(n\tau)\tau f_{xx}(k\tau+\tau-n\tau)+F_y(n\tau)\tau f_{xy}(k\tau+\tau-n\tau)\right.$$
$$\left.+F_z(n\tau)\tau f_{xz}(k\tau+\tau-n\tau)\right), \tag{13}$$

where $X(k\tau + \tau)$ denotes the response of the system at $k + 1$ in the x-direction, τ is the discrete time, k is the number of iterations. f_{ij} represents a unit IRF within a given bandwidth that contains all modal information within the selected bandwidth, the subscripts i and j represent the response in the i-direction caused by the excitation in the j-direction. Similarly, the response expressions for the y, z, directions can be obtained as follows:

$$Y(k\tau+\tau)=\sum_{n=1}^{k}\left(F_x(n\tau)\tau f_{yx}(k\tau+\tau-n\tau)+F_y(n\tau)\tau f_{yy}(k\tau+\tau-n\tau)\right.$$
$$\left.+F_z(n\tau)\tau f_{yz}(k\tau+\tau-n\tau)\right)Z(k\tau+\tau)=\sum_{n=1}^{k}\left(F_x(n\tau)\tau f_{zx}(k\tau+\tau-n\tau)\right.$$
$$+F_y(n\tau)\tau f_{zy}(k\tau+\tau-n\tau)$$
$$\left.+F_z(n\tau)\tau f_{zz}(k\tau+\tau-n\tau)\right). \tag{14}$$

The three-direction vibration response of robot based on IRF method and mode coupling effect can be rewritten as follows:

$$\begin{cases} X_{k+1}=\sum_{n=1}^{k}\left[\Psi^n_{xx,k+1}+\Psi^n_{xy,k+1}+\Psi^n_{xz,k+1}\right] \\ Y_{k+1}=\sum_{n=1}^{k}\left[\Psi^n_{yx,k+1}+\Psi^n_{yy,k+1}+\Psi^n_{yz,k+1}\right], \\ Z_{k+1}=\sum_{n=1}^{k}\left[\Psi^n_{zx,k+1}+\Psi^n_{zy,k+1}+\Psi^n_{zz,k+1}\right] \end{cases} \tag{15}$$

where

$$\Psi^n_{ij,k+1}=F_i(n\tau)\tau f_{ij}(k\tau+\tau-n\tau). \tag{16}$$

The iterative process solving Eq. (8) and Eq. (15) is expressed in graphs, as shown in Fig. 16. Firstly, the response signal of the k+1 step $x_{lev,ij}((k+1)\tau), y_{lev,ij}((k+1)\tau), z_{lev,ij}((k+1)\tau)$ is calculated by using the cutting force and IRF of the previous k step. Then, according to the vibration response signal at this time, the coordinates of the current blade point $(x_{T,ij}((k+1)\tau), y_{T,ij}((k+1)\tau))$ and the cutting interference point $(x_{T,ij,n}((k+1)\tau), y_{T,ij,n}((k+1)\tau))$ are calculated according to Eq. (3) and

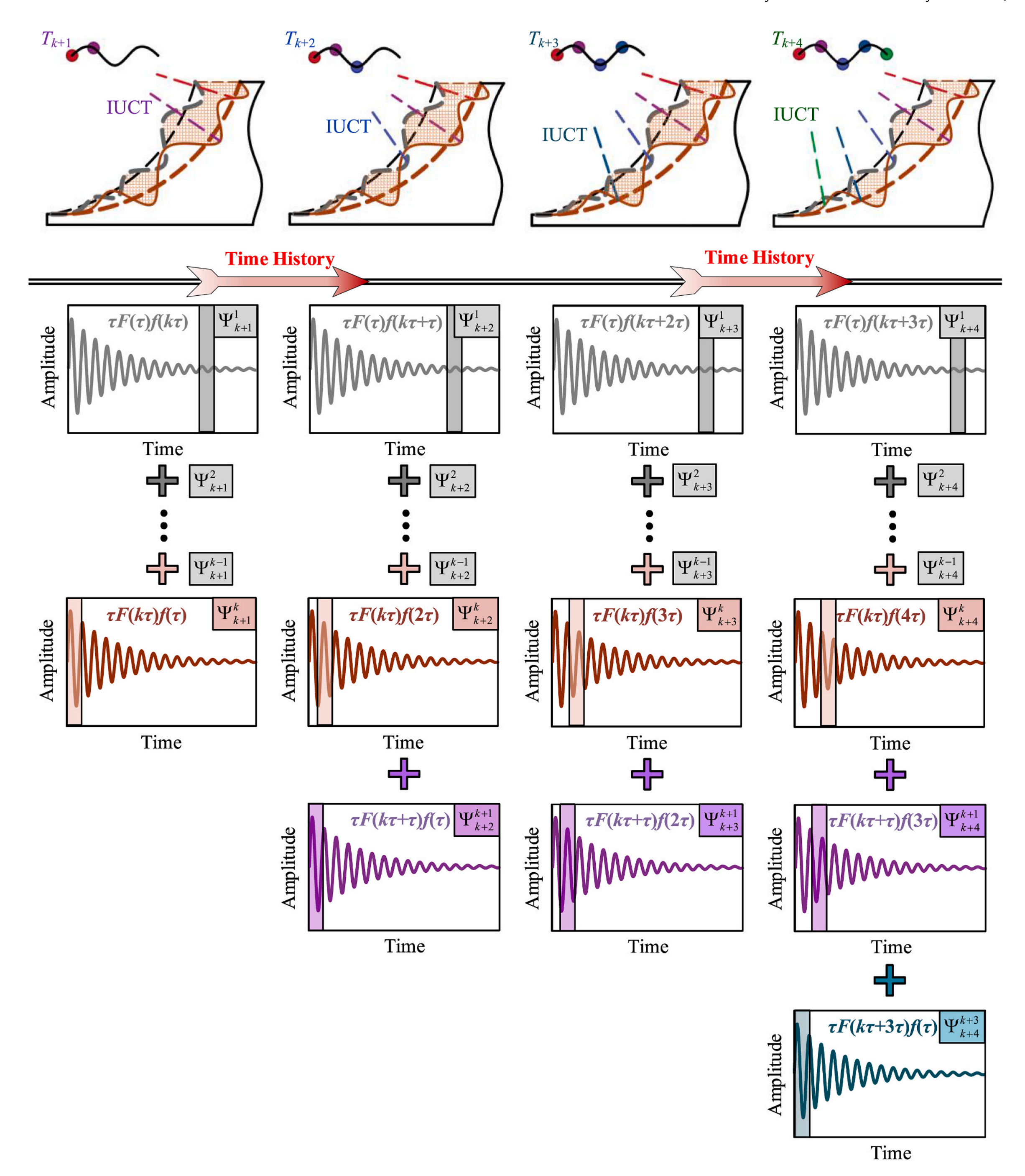


Fig. 16. Schematic diagram of vibration response solving process based on IRF. (IUCT means instantaneous uncut chip thickness.) The calculation rules of IRF method are as follows: T_{k+1} step is in normal cutting state; T_{k+2} step is in tool-workpiece separation state, the cutting force is zero; T_{k+3} step is in normal cutting state, but because of the influence of T_{k+2} step, a T_{k+2} step component needs to be reduced in the vibration calculation; T_{k+4} step is in normal cutting state, but the influence of T_{k+2} step also exists and needs to be taken into account in vibration calculation.

Eq. (4). Eq. (6) is used to judge whether cutting occurs at present. In this case, Eq. (8) can be used to calculate the current cutting force $F_x((k+1)\tau), F_y((k+1)\tau)$, $F_z((k+1)\tau)$ and update the cutting interference point $(x_{T.ij,k+1}(t), y_{T.ij,k+1}(t))$ according to the blade point coordinates at this time. If no cutting occurs, then the cutting force is zero and the cutting interference points on the workpiece surface do not need to be updated.

Fig. 16 depicts the calculation process of step T_{k+1}. In this step, there is no tool-workpiece separation occurs in the previous k step, and the vibration response calculation can be determined using Eq. (15). The cutting interference points on the workpiece surface are updated accordingly, and the vibration displacement $x_{lev.ij}((k+1)\tau), y_{lev.ij}((k+1)\tau), z_{lev.ij}((k+1)\tau)$ and cutting force $F_x((k+1)\tau), F_y((k+1)\tau)$, $F_z((k+1)\tau)$ of step $k+1$ are calculated and obtained.

The calculation process of the T_{k+2} step is the same as that of the T_{k+1} step, and the equation of vibration response is as follows:

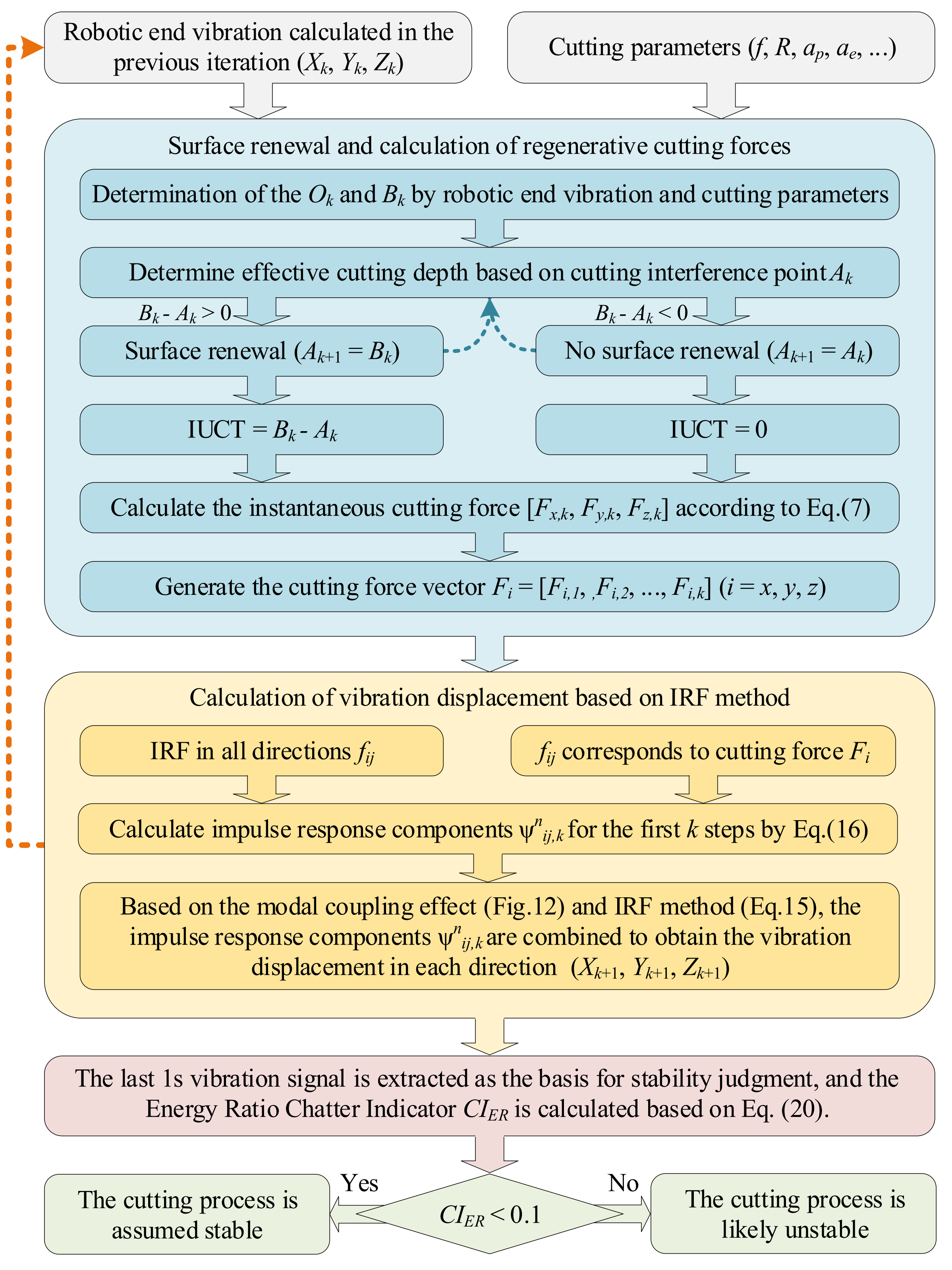


Fig. 17. Flowchart of LFC stability model, including stability analysis of simulation results.

Table 4
Simulation parameters for illustration.

Diameter (mm)	Tool teeth number	Helix angle (deg)	Feed per Tooth (mm)	Material	k_{tc} (N/mm^2)	k_{rc} (N/mm^2)	k_{ac} (N/mm^2)
25	3	7	0.05	NiAB	4940.2	5680.1	315.8

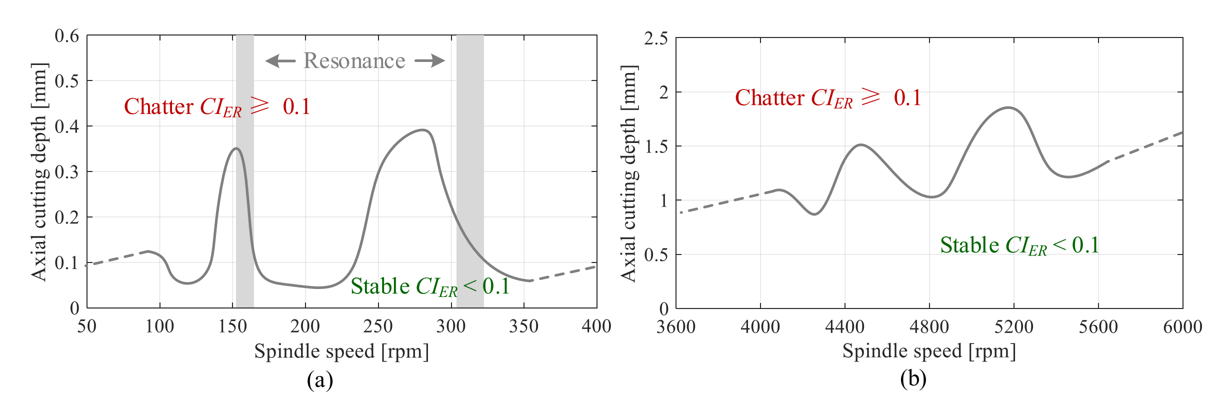


Fig. 18. Prediction results of milling stability under low-frequency chatter: (a) Stability prediction results at low speed region (Lobe order ≥1), (b) Stability prediction results at high speed region (Lobe order <1). The solid line of the figure is above the grid used for simulation, while the dashed line is not.

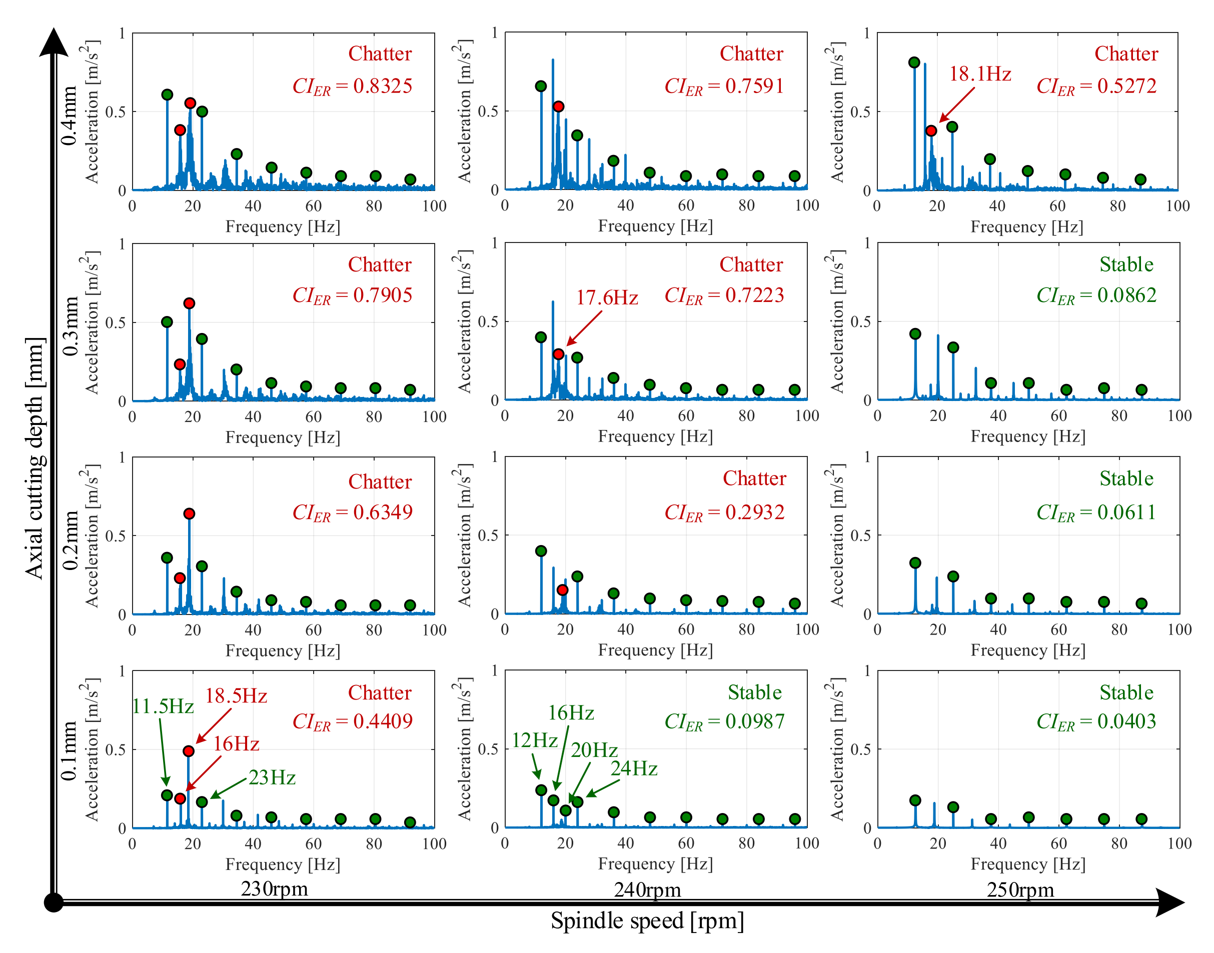


Fig. 19. Vibration spectrum of low-speed region (Lobe order ≥1).

$$\begin{cases} x_{lev,ij}((k+2)\tau) = \sum_{n=1}^{k+1}\left[\Psi^{n}_{xx,k+2} + \Psi^{n}_{yx,k+2} + \Psi^{n}_{zx,k+2}\right] \\ y_{lev,ij}((k+2)\tau) = \sum_{n=1}^{k+1}\left[\Psi^{n}_{xy,k+2} + \Psi^{n}_{yy,k+2} + \Psi^{n}_{zy,k+2}\right]. \\ z_{lev,ij}((k+2)\tau) = \sum_{n=1}^{k+1}\left[\Psi^{n}_{xz,k+2} + \Psi^{n}_{yz,k+2} + \Psi^{n}_{zz,k+2}\right] \end{cases} \tag{17}$$

According to Eq. (6), no cutting occurs. At this point, the cutting force is zero; there is no need to update the workpiece surface cutting interference point, and the vibration displacement $x_{lev,ij}((k+2)\tau), y_{lev,ij}((k+2)\tau), z_{lev,ij}((k+2)\tau)$ is calculated.

In the calculation of the T_{k+3} step, the cutting force of the T_{k+2} step is not needed to be considered in the vibration response calculation because the tool-workpiece separation occurs in the T_{k+2} step. However, the IRF is still consistent with the calculation step and needs to be iterated one step backward. The equation is as follows:

$$\begin{cases} x_{lev,ij}((k+3)\tau) = \sum_{n=1}^{k+2}\left[\Psi^{n}_{xx,k+3} + \Psi^{n}_{yx,k+3} + \Psi^{n}_{zx,k+3}\right] \\ y_{lev,ij}((k+3)\tau) = \sum_{n=1}^{k+2}\left[\Psi^{n}_{xy,k+3} + \Psi^{n}_{yy,k+3} + \Psi^{n}_{zy,k+3}\right], \\ z_{lev,ij}((k+3)\tau) = \sum_{n=1}^{k+2}\left[\Psi^{n}_{xz,k+3} + \Psi^{n}_{yz,k+3} + \Psi^{n}_{zz,k+3}\right] \end{cases} \tag{18}$$

where $\Psi^{k+2}_{ij,k+3} = 0$. Finally, the cutting force $F_x((k+3)\tau), F_y((k+3)\tau), F_z((k+3)\tau)$ is calculated according to Eq. (8), and the coordinates of cutting interference points on the workpiece surface are updated.

In the calculation of the T_{k+4} step, the cutting force of the T_{k+2} step is also not needed to be considered. The calculation expression is as follows:

$$\begin{cases} x_{lev,ij}((k+4)\tau) = \sum_{n=1}^{k+3}\left[\Psi^{n}_{xx,k+4} + \Psi^{n}_{yx,k+4} + \Psi^{n}_{zx,k+4}\right] \\ y_{lev,ij}((k+4)\tau) = \sum_{n=1}^{k+3}\left[\Psi^{n}_{xy,k+4} + \Psi^{n}_{yy,k+4} + \Psi^{n}_{zy,k+4}\right], \\ z_{lev,ij}((k+4)\tau) = \sum_{n=1}^{k+3}\left[\Psi^{n}_{xz,k+4} + \Psi^{n}_{yz,k+4} + \Psi^{n}_{zz,k+4}\right] \end{cases} \tag{19}$$

where $\Psi^{k+2}_{ij,k+4} = 0$. The cutting force is also calculated according to Eq. (8), and the cutting interference points on the workpiece surface are updated. The following iterative calculation process is analogous.

Using this information, we can simulate the vibration displacement, velocity, and acceleration signals of the robot end. In the early stage of cutting simulation, the actual radial cutting depth is less than the set value since the initial engagement condition of the tool and workpiece in the surface renewal model is not contact. Therefore, the cut path is greater than 12.5 mm. We set the feed per tooth to $f_z = 0.05$ mm, speed to n, and the number of teeth to N. The feed speed is calculated as $f = f_z nN/60$. The time to start recording simulation results is $t_{st} = 12.5/f$.

Since the modal frequency of the robot structure is low, the LFC caused by it also has a low-frequency (generally around 10–30 Hz). To better predict the occurrence of chatter, we collect a total of 1 s of vibration signals as the basis for the final stability judgment. Therefore, the time to finish recording simulation results is $t_{ex} = 1 + 12.5/f$. This ensures that possible chatter can be fully displayed.

The Energy Ratio Chatter Indicator [33,35] is used to calculate a quantitative stability index, CI_{ER}, based on the simulation results obtained in the last second. This enables us to quantitatively judge the stability, with CI_{ER} approaching 0 indicating stable processing and 1 indicating severe chatter. We set the threshold for stable and chatter state of the numerical simulation results at 0.1 based on the characteristics of CI_{ER}. The expression for CI_{ER} is as follows:

$$CI_{ER} = \frac{E_c}{E} = 1 - \frac{E_p + E_n}{E}, \tag{20}$$

where E is the energy of the vibration signal, E_c is the energy of the aperiodic component of the vibration signal caused by chatter, E_p is the energy of the periodic component of the vibration signal (including the rotation frequency, tooth-passing frequency and their harmonic frequency), and E_n is the energy of the aperiodic component caused by environmental noise. Since there is no environmental noise in the numerical simulation, the corresponding CI_{ER} can be simplified as follows:

$$CI_{ER} = \frac{E_c}{E} = 1 - \frac{E_p}{E}, \tag{21}$$

therefore, we have the following stability judgment indicators:

$$\begin{cases} CI_{ER} < 0.1 \quad \text{Stable} \\ 0.1 \le CI_{ER} \le 1 \quad \text{Chatter} \end{cases}. \tag{22}$$

To sum up, the calculation flowchart of LFC stability model can be summarized as shown in Fig. 17.

3.3. Simulation and analysis

We use the LFC stability model to comprehensively consider the modulated tool-workpiece engagement conditions and the mode coupling effect of the robot structure, and calculate the LFC stability boundary of lobe order ≥1 (100–350 rpm, referred to as the low speed region) and lobe order <1 (4000–5600 rpm, referred to as the high speed region). The distribution of simulation parameters in the low speed region ranges from 100 to 350 rpm (with a 10 rpm interval) and 0.1–0.5 mm (with a 0.1 mm interval), while the distribution of simulation parameters in the high speed region ranges from 4000 to 5600 rpm (with a 200 rpm interval) and 0.6–2.0 mm (with a 0.2 mm interval). A bull-nosed tool (600-025A25-10H) is used in the simulation. The cutting force coefficients in Table 4 are identified by cutting experiments [36]. The radial cutting depth used in the simulation is 12 mm. Each group is numerically simulated using the flowchart shown in Fig. 17. A simulation result with $CI_{ER} \ge 0.1$ is defined as chatter, while a result with $CI_{ER} < 0.1$ is defined as stable. The stability boundary is drawn accordingly, as shown in Fig. 18. The acceleration spectrum in typical regions ((230–250 rpm) × (0.1–0.4 mm) and (5000–5400 rpm) × (1.2–1.8 mm)) is shown in Figs. 19 and 20.

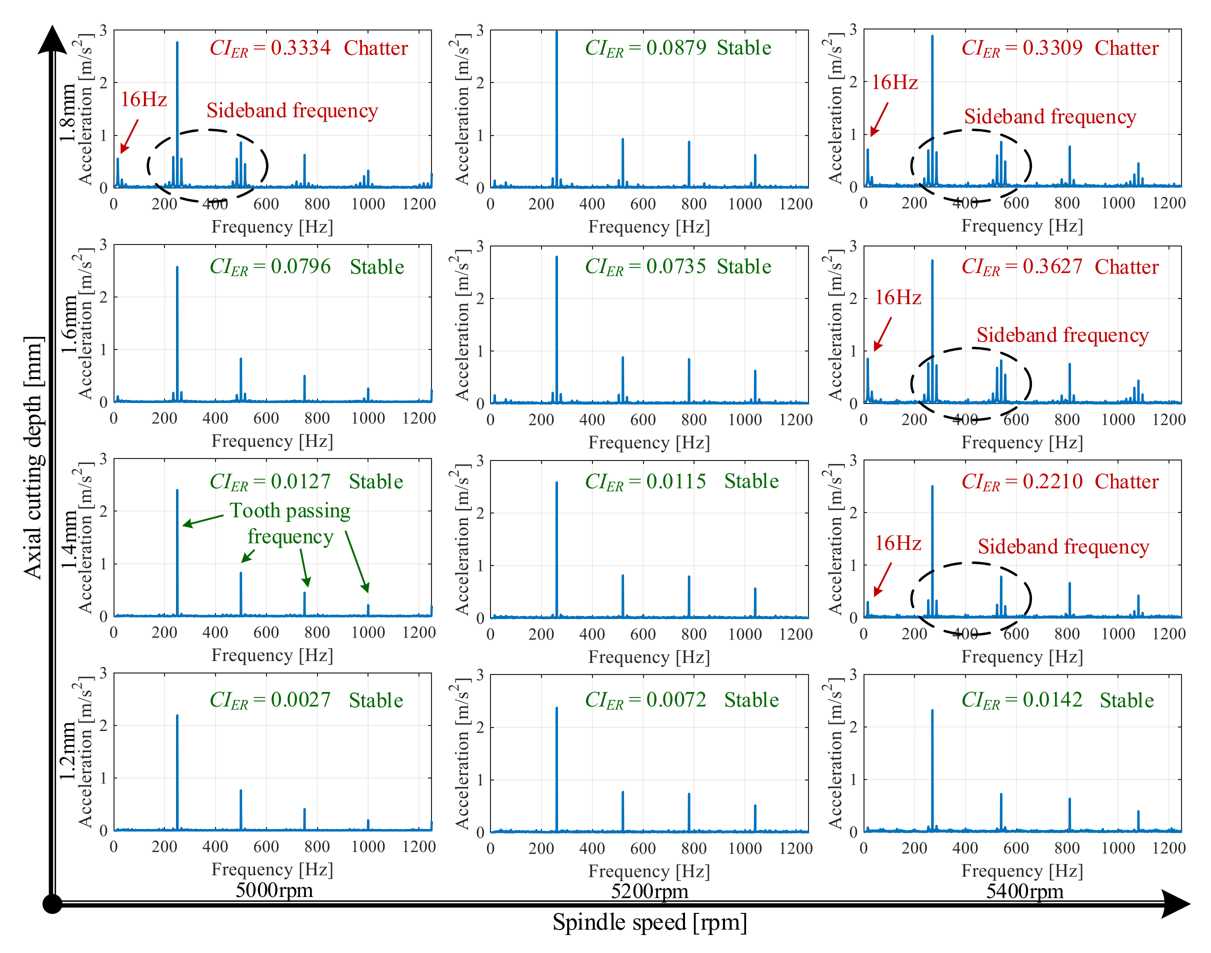


Fig. 20. Vibration spectrum of high-speed region (Lobe order <1).

During the simulation calculation, low-frequency vibrations were observed to exhibit sideband phenomenon, particularly in the high speed region, which is similar to the sideband signal depicted in Fig. 3b. The appearance of this phenomenon in the simulation provides further support for using the sideband signal as the characteristic signal for detecting low-frequency vibration. However, the sideband phenomenon poses a challenge for conventional milling vibration signal analysis, and it also produces additional high-frequency vibration marks on the workpiece surface. Despite these difficulties, active vibration control in robotic milling can effectively demodulate the low-frequency vibration signals using the sideband signal to achieve targeted vibration suppression.

The simulation results indicate that the chatter frequency is close to the first-order modal frequency of the robot, which is approximately 16 Hz. The stability boundary obtained by simulation exhibits spindle speed dependence, which further confirms the impact of regenerative effect on LFC in robotic milling. Hence, the occurrence of LFC in robotic milling can be attributed to factors such as poor dynamic stiffness, low modal frequency, and mode coupling effect. Additionally, the modulated tool-workpiece engagement conditions lead to a correlation between critical axial cutting depth and spindle speed. These factors together contribute to the formation of the stability lobe diagram as shown in Fig. 18.

Fig. 21 shows that LFC occurs at 5400 rpm when the axial cutting depth is 1.6 mm and the radial cutting depth is 8 mm. The vibration trajectory under these conditions is depicted in Fig. 22. At the beginning of cutting, the tool tip experiences significant shifts due to the weak rigidity of the robot. This shift, which is caused by the overall translation deformation of the tool resulting from the deformation of the robot structure, is not to be confused with the deformation of the tool itself.

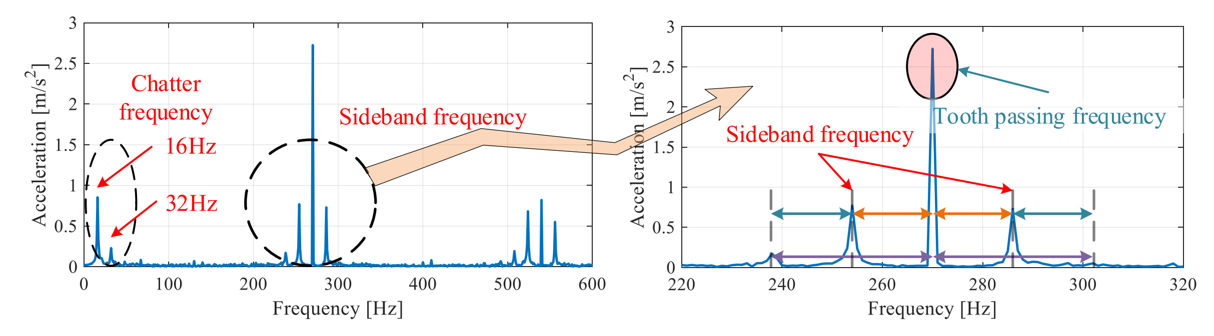


Fig. 21. Low-frequency chatter and sideband phenomenon. Low-frequency vibration and forced vibration are modulated to form sideband frequency.

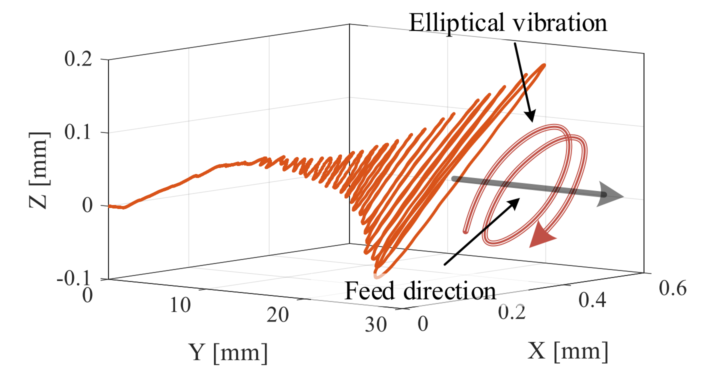


Fig. 22. Vibration trajectory of the tool tip in chatter state. Due to the poor stiffness, the end of the robot will first have a large shift, and then the chatter components in the vibration gradually diverge, and finally form a typical elliptical vibration trajectory.

The direction of cutting force in milling is time-varying, and when it is not orthogonal to the mode direction, a new cutting force is generated that excites the mode. The vibration of any mode affects itself and its adjacent modes as the cutting process progresses, due to the combined effect of force-position feedback and mode coupling. This leads to the formation of LFC with elliptical vibration characteristics, as shown in Fig. 22.

To compare the accuracy of the proposed LFC stability model with other methods, we adopt the Multi-Frequency Approximation (MFA) mode coupling stability prediction method from Refs. [23,37] which only considers the mode coupling effect, and the FDM, which only considers the regenerative effect. The MFA method is used with settings consistent with reference [23], with the number of harmonics set to the maximum value and changed based on the selected spindle speed and maximum frequency, which is set to 1000 Hz. We substitute the same parameters (IRF and its corresponding modal parameters, where the modal parameters are shown in Table A1 in Appendix A.), and compare the prediction results of the three models in Fig. 23. In the low-speed region (lobe order ≥1), the stability boundary predicted by the LFC method is close to that predicted by the FDM model, which only considers the regenerative effect. However, there is a significant difference between the stability boundary predicted by the MFA model, which only considers the mode coupling effect. In the high-speed region (lobe order <1), the stability boundary predicted by the LFC method is clearly different from that predicted by the models that only consider the regenerative or mode coupling effects. When only the mode coupling effect is considered, the critical cutting depth remains constant with spindle speed, and the stability limit is low, as shown by the orange dashed line in the figure. When only the regenerative effect is considered, the critical cutting depth changes with spindle speed, but the stability boundary predicted by the model is obviously too high in the high-speed region, as shown by the blue dotted line in the figure. When both the mode coupling and regenerative effects are considered simultaneously, the stability boundary exhibits a lobe shape as the speed changes, as shown by the solid gray line in the figure. To verify the accuracy of the stability prediction, we conduct stability experimental verification and analysis in Section 4 (see Fig. 25).

4. Experimental verification and discussion of sideband phenomenon

In order to verify the accuracy of mechanism analysis and model establishment in Section 3, a robotic milling stability verification experiment is carried out in this section. And the reason of sideband phenomenon is deduced theoretically. Experimental video and

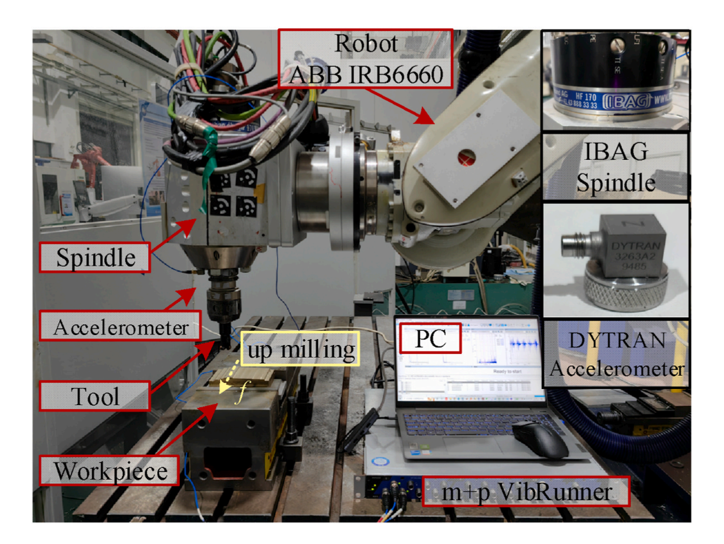
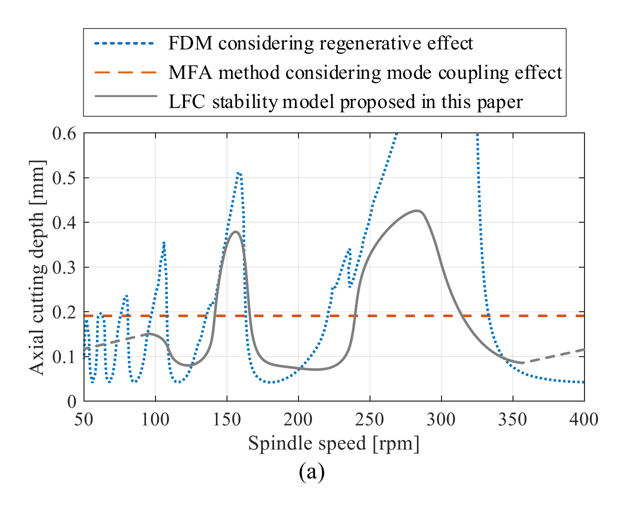


Fig. 24. Robotic milling experimental equipment.



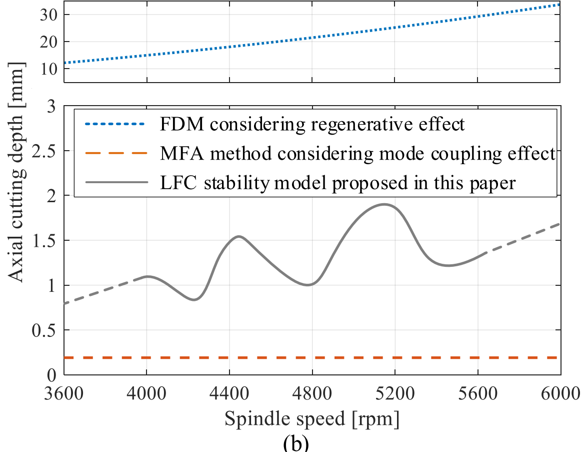


Fig. 23. Comparison of prediction results of each model: (a) Low speed region (Lobe order ≥1), (b) High speed region (Lobe order <1). Multi frequency approximation (MFA) method and full-discretization method (FDM) are used as comparison methods, respectively. In the low speed region, FDM is close to the predicted results of the proposed method, while in the high speed region, there is an unreasonable increase exponentially in the stability boundary. The MFA method shows the lowest stability boundary independent of spindle speed in all regions. By contrast, the proposed method shows a reasonable speed dependence in all ranges, and the prediction results are more consistent with cognition in the high speed region.

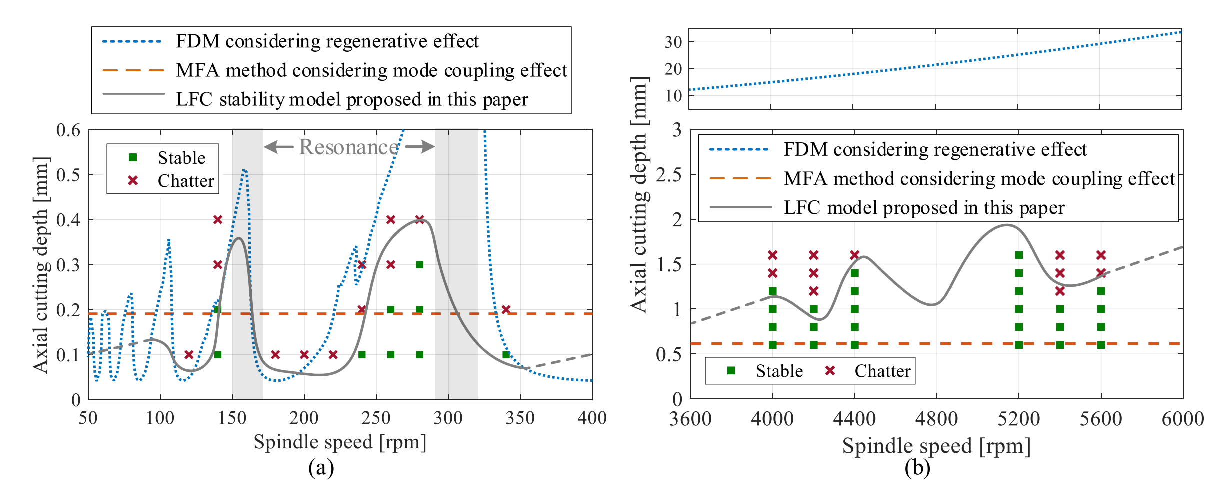


Fig. 25. Comparison of milling stability experiment and simulation: (a) Low speed region (lobe order ≥1), (b) High speed region (lobe order <1). Multi frequency approximation (MFA) method and full-discretization method (FDM) are used as comparison methods, respectively. For the prediction of LFC stability boundary, both FDM and the proposed LFC method have certain accuracy in the low speed region, and the LFC method is closer to the experiment at the peak of the stability lobe diagram, while in the high speed region, only the prediction result of the LFC method is close to the experiment, and other methods cannot be applied.

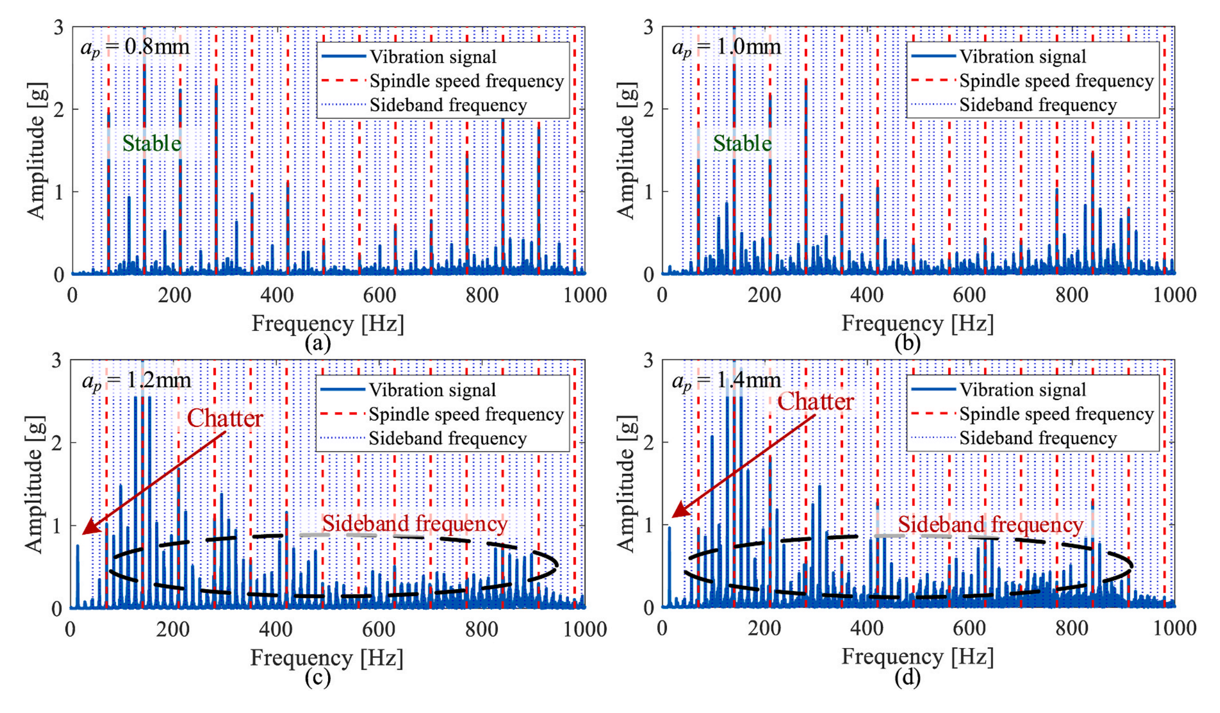


Fig. 26. Spectrum of vibration acceleration at 4200 rpm. (a) $a_p = 0.8$ mm; (b) $a_p = 1.0$ mm; (c) $a_p = 1.2$ mm; (d) $a_p = 1.4$ mm. The significant chatter signal in the low-frequency of the spectrum and clear sideband frequencies in the whole band indicate the occurrence of low-frequency chatter.

mechanism demonstration animation of low-frequency chatter can be seen in the Video 1 in Appendix B.

Supplementary video related to this article can be found at https://doi.org/10.1016/j.ijmachtools.2023.104048

4.1. Experimental verification and comparison

Fig. 24 displays the robotic milling experimental equipment used in this study, which consists of an ABB IRB6660 robot and an IBAG HF170 spindle. The material used for the experiment was nickel-aluminum bronze, and up milling was used as the milling type. A bull-nosed cutting tool (600-025A25-10H) was chosen with an overhang length of 60 mm, selecting the shortest overhang length within the optional range to maximize the tool rigidity. Table 4 provides additional relevant parameters. The radial cutting depth was determined to be 12 mm, and the feed per tooth was set at 0.05 mm/rev/tooth. Milling stability verification experiments were conducted in the low-speed region of lobe order ≥1 (120−340 rpm) and the high-speed region of lobe order <1 (4000−5600 rpm). The acceleration sensor (DYTRAN Model: 3263A2, S/N: 9485) was used to measure the vibration signals. Considering that the vibration source of LFC is located in the robotic structure, the spindle at the end of the robot is the best measurement position, so the sensor was installed at the spindle at the end of the robot. The m + p Vibrunner was the data acquisition system, and the sampling frequency was set at 4096 Hz. It was assumed that the structural modal of the robot in the experimental cutting path with 70 mm did not change due to small changes in robotic posture. A comparison between stability prediction and experiment is shown in Fig. 25.

Fig. 26 depicts the acceleration spectrum at a spindle speed of 4200 rpm (lobe order ≈ 0.076) and a cutting depth of 0.8–1.4 mm. It is

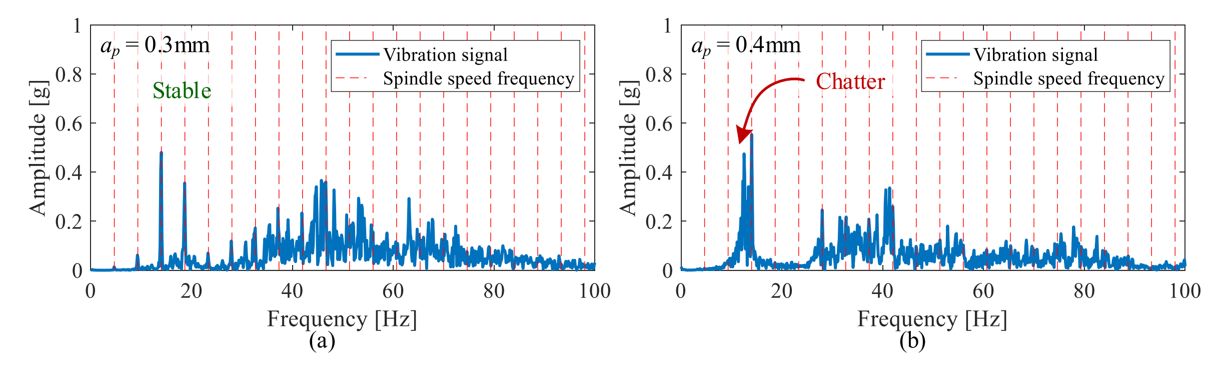


Fig. 27. Spectrum of vibration acceleration at 280 rpm: (a) $a_p = 0.3$ mm; (b) $a_p = 0.4$ mm. Compared with the spectrum signals of the chatter state in the high speed region (lobe order <1), the low speed region (lobe order ≥1) is closer to the regenerative chatter in heavy-duty machining, including the strong low-frequency forced vibration and the energy concentration near the chatter frequency.

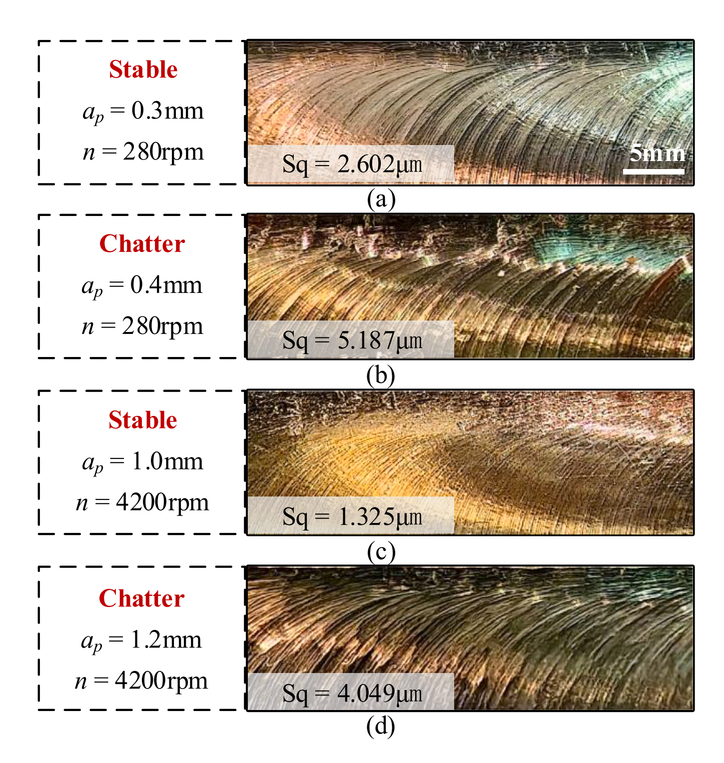


Fig. 28. Surface morphology under different machining parameters. (a) a_p = 0.3 mm, n = 280 rpm, Sq = 2.602 μm, stable. (b) a_p = 0.4 mm, n = 280 rpm, Sq = 5.187 μm, chatter. (c) a_p = 1.0 mm, n = 4200 rpm, Sq = 1.325 μm, stable. (d) a_p = 1.2 mm, n = 4200 rpm, Sq = 4.049 μm, chatter. When chatter occurs, there are very obvious marks of low-frequency vibration on the workpiece surface. However, because the low-frequency forced vibration is larger at low spindle speed, it seems that there are also relatively obvious marks of low-frequency vibration in figure (a). At this time, it is necessary to observe the components of the frequency spectrum to conclude that this is a stable processing state.

evident from the figure that a severe low-frequency vibration occurs when the axial cutting depth is increased to 1.2 mm. Significant sideband phenomena around the tooth-passing frequencies and their multiples are also visible, indicating the occurrence of LFC. When LFC occurs during robotic milling, the workpiece surface exhibits visible vibration marks with characteristic chatter frequency. To illustrate this, the processed surfaces with axial cutting depths of 1.0 mm and 1.2 mm are displayed in Fig. 28c and d, respectively. A clear contrast is evident between the high-quality surface without chatter and the surface with obvious vibration marks caused by chatter. Fig. 27 displays the acceleration spectrum at a spindle speed of 280 rpm (lobe order ≈ 1.14) and an axial cutting depth of 0.3–0.4 mm. When no chatter occurs, only the tooth-passing frequency and its harmonic frequency exist in the low-frequency range of 0∼20 Hz. However, when chatter occurs, as shown in Fig. 27b, there is significant energy concentration and LFC frequency in the low-frequency range, indicating the occurrence of LFC. Correspondingly, the surface morphology is shown in Fig. 28, and the surface roughness is 2.602 μm, 5.187 μm, 1.325 μm, and 4.049 μm, respectively.

To better observe the impact of LFC on the workpiece surface, we conducted surface morphology testing using a Zeiss confocal microscope (Smartproof 5). Fig. 29a presents a three-dimensional view of the surface morphology in the stable state, while Fig. 29b displays the three-dimensional view of the surface morphology in the chatter state. As depicted in Fig. 29a, the surface without chatter exhibits fine and dense machining marks with around 20 peaks and troughs visible in the 1 mm processing path. At a feed per tooth of 0.05 mm and a feed speed of 10.5 mm/s at 4200 rpm, the forced vibration frequency is 210 Hz, consistent with the observed results. On the other hand, Fig. 29b shows the surface with chatter, where two distinct low-frequency vibration marks appear in addition to the dense machining marks. The peak-to-peak distance is about 0.6–0.7 mm, and the vibration frequency is approximately 15–17.5 Hz, close to the robot's modal frequency. Hence, it can be concluded that severe LFC occurs at this point.

The stability boundary of robotic milling experiments is found to have a significant dependence on the spindle speed. However, when considering the mode coupling effect and regenerative effect comprehensively, stability prediction is possible by combining the SR model, which yields results close to the experimental results. The acceleration spectra of spindle speed of 4200 rpm and cutting depth of 0.8–1.4 mm, and spindle speed of 280 rpm and cutting depth of 0.3–0.4 mm are shown in Figs. 26 and 27, respectively. On the other hand, when only the mode coupling effect is considered, the stability prediction result is independent of the spindle speed, leading to significant discrepancies between the predicted and experimental results, similar to Fig. 8 in Ref. [23]. Similarly, when only the regenerative effect is considered, the traditional regenerative chatter stability model fails to account for the complete dynamic chip thickness change due to the tooth-passing frequency being much larger than the mode frequency. Without accounting for the influence of the mode coupling effect, the stability boundary becomes extremely high and increases with the increase of spindle speed, similar to the predicted results of Mode 1,2 of Fig. 5 in Ref. [8]. In such cases, the stability prediction results also have a large error.

In this section, we conduct a milling experiment to verify the stability model's accuracy by comparing its predictions when only considering the mode coupling effect, only considering the regenerative effect, and considering both types of self-excited vibration effects simultaneously. The experimental results confirm that both regenerative and mode coupling effects need to be considered together to accurately predict LFC in robotic milling. The dynamic cutting force in milling depends on the interaction between previous and current vibrations. Since the rotary tool always cuts the previously cut workpiece surface when removing material from the workpiece, it is necessary to consider the regenerative

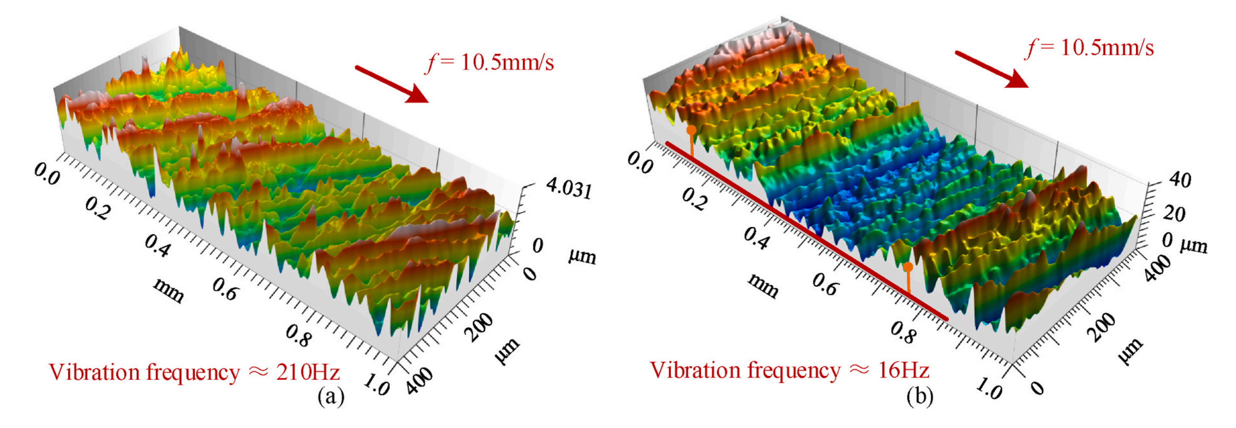


Fig. 29. Three-dimensional view of surface morphology. (a) $a_p = 1.0$ mm, $n = 4200$ rpm, Sq = 1.325 μm, stable. (b) $a_p = 1.2$ mm, $n = 4200$ rpm, Sq = 4.049 μm, chatter. According to the feed speed, it can be estimated that the frequency of large vibration in Figure (b) is about 16Hz, which is close to the natural frequency of the robotic mode.

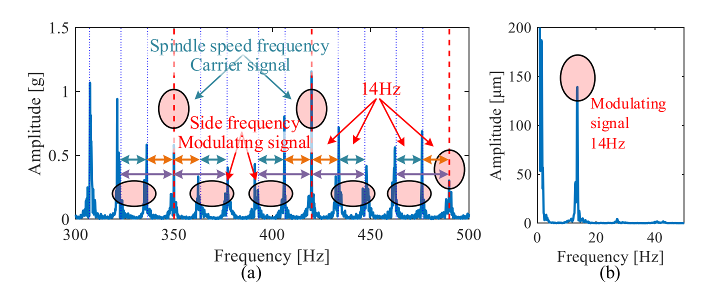


Fig. 30. Sideband phenomenon in robotic milling: (a) Acceleration spectrum diagram, (b) Displacement spectrum diagram.

effect. The robot structure has poor rigidity and complex modal characteristics, with 2–4 modes at 10–30 Hz and significant interaction between each mode, forming a force-position feedback between the modes and the mode coupling effect. Therefore, both effects need to be considered. Furthermore, as analyzed in Section 2.2, the regenerative effect's consideration in LFC needs to be adjusted accordingly (modulated tool-workpiece engagement conditions). Neglecting any of these factors can lead to errors in stability prediction. Thus, the proposed LFC stability model integrates the modulated tool-workpiece engagement conditions and mode coupling effect to achieve accurate stability prediction of LFC in robotic milling.

During the milling experiments, sideband phenomenon and LFC occur simultaneously. The regular sideband signal is distributed around the tooth-passing frequencies and their multiples with the LFC frequency as the frequency interval. Slightly different from the simulated acceleration spectrum, the measured spectrum in the milling experiment includes not only the tooth-passing frequencies and their multiples but also the rotation frequencies and their multiples. Therefore, the sideband also forms around the rotation frequencies and their multiples. The occurrence of the sideband is closely related to the low-frequency vibration. To clarify this relationship, we deduce and simulate the causes of the sideband phenomenon in the following section.

4.2. Mathematical derivation and discussion of sideband phenomenon

Sideband is not a common phenomenon in machine tool milling and is observed in the acceleration spectrum of robotic milling with low-frequency vibration. By observing the acceleration spectrum, it can be found that with the occurrence of low-frequency vibration, there will be many sideband signals with regular distribution around the rotation frequencies, tooth passing frequencies and their multiples. The interval frequency is the low-frequency vibration frequency and the interval frequency changes with the change of the low-frequency vibration frequency. The spectrum details are shown in Fig. 30.

The frequency interval of the sideband signal is consistent with the frequency of low-frequency vibration, and the sideband signal exists around each of the rotation frequencies, tooth passing frequencies, and their multiples. This phenomenon has the same characteristics as the sideband signal in gear and bearing fault diagnosis [30]. This sideband modulation phenomenon is an obstacle to milling vibration signal processing, but it can also be used as the characteristic signal of low-frequency vibration of robotic milling. Based on the research of sideband phenomenon in gear and bearing fault diagnosis, this section analyzes sideband phenomenon based on cutting force modulation and explains the cause and evolution law of sideband phenomenon in robotic milling.

Firstly, the instantaneous cutting force model is established as follows:

$$\begin{cases} F_x(t) = -\sum_{i=1}^{N}\sum_{j=1}^{M} g(\varphi_{ij})h(\varphi_{ij})\left[k_{tc}\cos(\varphi_{ij}) + k_{rc}\sin(\varphi_{ij})\right]dz \\ F_y(t) = \sum_{i=1}^{N}\sum_{j=1}^{M} g(\varphi_{ij})h(\varphi_{ij})\left[k_{tc}\sin(\varphi_{ij}) - k_{rc}\cos(\varphi_{ij})\right]dz \\ F_z(t) = -\sum_{i=1}^{N}\sum_{j=1}^{M} g(\varphi_{ij})h(\varphi_{ij})k_{ac}dz \end{cases} \tag{23}$$

When the dynamic chip thickness is considered, the cutting force expression is shown as follows:

$$\begin{cases} F_x(t) = -\sum_{j=1}^{N}\sum_{i=1}^{\tilde{M}} g(\varphi_{ij})\tilde{h}(\varphi_{ij})\left[k_{tc}\cos(\varphi_{ij}) + k_{rc}\sin(\varphi_{ij})\right]dz \\ F_y(t) = \sum_{j=1}^{N}\sum_{i=1}^{\tilde{M}} g(\varphi_{ij})\tilde{h}(\varphi_{ij})\left[k_{tc}\sin(\varphi_{ij}) - k_{rc}\cos(\varphi_{ij})\right]dz \\ F_z(t) = -\sum_{j=1}^{N}\sum_{i=1}^{\tilde{M}} g(\varphi_{ij})\tilde{h}(\varphi_{ij})k_{ac}dz \end{cases} \tag{24}$$

where ,

$$\begin{cases} \tilde{M} = M + \dfrac{\Delta Z}{dz} \\ \tilde{h}(\varphi_{ij}) = h(\varphi_{ij}) + \Delta X\sin\varphi_{ij} + \Delta Y\cos\varphi_{ij} \end{cases} \tag{25}$$

considering only the dynamic change, the dynamic cutting force is shown below:

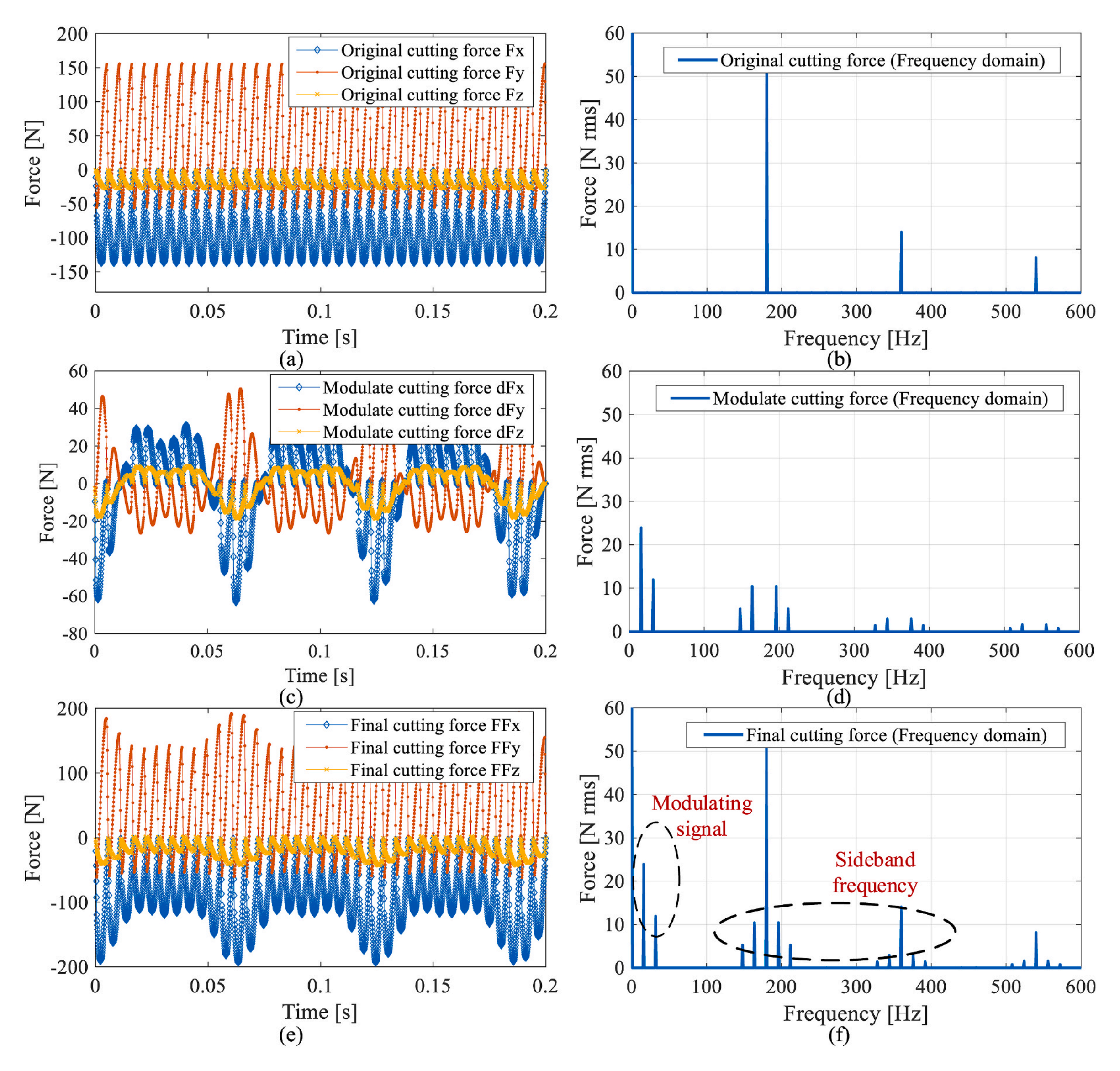


Fig. 31. Simulation of cutting force modulation phenomenon considering low-frequency vibration of the robot: (a) Original cutting force, (b) Modulate cutting force, (c) Final cutting force.

$$\begin{cases} \Delta F_x(t) = -\sum_{j=1}^{N}\sum_{i=1}^{\tilde{M}}\left[g(\varphi_{ij})\left(\Delta X \sin\varphi_{ij} + \Delta Y \cos\varphi_{ij}\right)\left(k_{tc}\cos(\varphi_{ij}) + k_{rc}\sin(\varphi_{ij})\right)dz\right] - \sum_{j=1}^{N}\sum_{i=M}^{\tilde{M}}F_x(t) \\ \Delta F_y(t) = \sum_{j=1}^{N}\sum_{i=1}^{\tilde{M}}\left[g(\varphi_{ij})\left(\Delta X \sin\varphi_{ij} + \Delta Y \cos\varphi_{ij}\right)\left(k_{tc}\sin(\varphi_{ij}) - k_{rc}\cos(\varphi_{ij})\right)dz\right] + \sum_{j=1}^{N}\sum_{i=M}^{\tilde{M}}F_y(t) \\ \Delta F_z(t) = -\sum_{j=1}^{N}\sum_{i=1}^{\tilde{M}}\left[g(\varphi_{ij})\left(\Delta X \sin\varphi_{ij} + \Delta Y \cos\varphi_{ij}\right)k_{ac}dz\right] - \sum_{j=1}^{N}\sum_{i=M}^{\tilde{M}}F_z(t) \end{cases} \tag{26}$$

If chatter does not occur, the amplitude of low-frequency vibration is generally from microns to tens of microns. However, the common axial cutting depth in robot milling is about $Z \approx 1{\sim}3$ mm. Therefore, a formula $\Delta Z/dz \ll Z/dz = M$ exists, and it can be known that Z-direction vibration has little influence on the cutting force and can be approximately ignored. Then, Eq. (26) can be simplified as:

$$\begin{cases} \Delta F_x(t) = \sum_{j=1}^{N}\sum_{i=1}^{M} g(\varphi_{ij})\left(\Delta X \sin\varphi_{ij} + \Delta Y \cos\varphi_{ij}\right)K_{x,ij}dz \\ \Delta F_y(t) = \sum_{j=1}^{N}\sum_{i=1}^{M} g(\varphi_{ij})\left(\Delta X \sin\varphi_{ij} + \Delta Y \cos\varphi_{ij}\right)K_{y,ij}dz \\ \Delta F_z(t) = \sum_{j=1}^{N}\sum_{i=1}^{M} g(\varphi_{ij})\left(\Delta X \sin\varphi_{ij} + \Delta Y \cos\varphi_{ij}\right)K_{z,ij}dz \end{cases} \tag{27}$$

Table 5
Simulation parameters for illustration.

Item	Value
Tool diameter (mm)	12
Tool teeth number	3
Tool helix angle (deg)	30
k_{tc} **(N/mm²)**	796.1
k_{rc} **(N/mm²)**	168.8
k_{ac} **(N/mm²)**	222.0
Axial cutting depth (mm)	2
Radial cutting depth (mm)	8
Spindle speed (rpm)	3600
Feed per tooth (mm)	0.0556

where,

$$\begin{cases} K_{x,ij} = -k_{tc}\cos(\varphi_{ij}) - k_{rc}\sin(\varphi_{ij}) \\ K_{y,ij} = k_{tc}\sin(\varphi_{ij}) - k_{rc}\cos(\varphi_{ij}) \\ K_{z,ij} = -k_{ac} \end{cases} \tag{28}$$

Eq. (23) and Eq. (27) respectively represent the equations of cutting force without and with consideration of low-frequency vibration. Combining Eq. (23) and Eq. (27), the ratio of the additional cutting force due to low-frequency vibration to the original cutting force is as follows:

$$\frac{\Delta F_x}{F_x} = \frac{\Delta F_y}{F_y} = \frac{\Delta F_z}{F_z} = \frac{\Delta X\sin\varphi_{ij} + \Delta Y\cos\varphi_{ij}}{h(\varphi_{ij})} = \frac{\Delta X\sin\varphi_{ij} + \Delta Y\cos\varphi_{ij}}{f_z\cos\varphi_{ij}} = A_x\tan\varphi_{ij} + A_y \tag{29}$$

describe it in matrix form:

$$\begin{bmatrix} \Delta F_x \\ \Delta F_y \\ \Delta F_z \end{bmatrix} = (A_x\tan\varphi_{ij} + A_y)\begin{bmatrix} F_x \\ F_y \\ F_z \end{bmatrix} \tag{30}$$

where,

$$\begin{cases} A_x = \Delta X / f_z \\ A_y = \Delta Y / f_z \end{cases} \tag{31}$$

A_x, A_y are the increased ratio of cutting force caused by low-frequency vibration, respectively. f_z represents the feed per tooth and is a constant at this time. $\Delta X, \Delta Y$ represent the components of the low-frequency vibration in the X and Y directions, which is a periodic function with a certain frequency and amplitude.

For ΔF affected by low-frequency vibration, the above phenomenon is expressed as the amplitude multiplied of the original cutting force signal and the low-frequency vibration signal at each point, that is, the product of the two signals in the time domain (e.g., $F_x \cdot \Delta X$), which is expressed as the convolution in the frequency domain (e.g., $\mathscr{F}(F_x) * \mathscr{F}(\Delta X)$). Frequency domain convolution computations "carry" the low-frequency signal around the high-frequency signal, which is the modulation phenomenon. Finally, the change of cutting force brings about the change of vibration, which is the cause of the sideband signal in the vibration signal. This phenomenon also exists in the milling of thin-walled parts [38], but because of the high modal frequency of thin-walled parts, it is difficult to observe a clear sideband frequency signals such as the robotic low-frequency chatter.

In the robotic milling process, when the low-frequency vibration amplitude is only 20 μm, the changes of time and frequency domain signals in the cutting force are shown in Fig. 31. Figs. 31a and b are original cutting force signals, Figs. 31c and d are modulated cutting force signals under the influence of low-frequency vibration of the robotic milling, Figs. 31e and f are final cutting force signals. Simulation parameters are shown in Table 5.

As shown in Fig. 31b, when the low-frequency vibration is not considered, only the tooth passing frequencies and their multiples exist in the cutting force signal. When low-frequency vibration occurs, the vibration signal will be modulated with the original cutting force signal, and the low-frequency signal and sideband signal appear simultaneously, as shown in Fig. 31d. The final cutting force is the superposition of those, as shown in Fig. 31f.

In conclusion, the appearance of sideband signal in robotic milling is due to the modulation of low-frequency vibration signal and forced vibration signal. In the study of signal analysis, modulation and demodulation can be used to extract and analyze signals. On the other hand, the sideband signal can be used as the characteristic signal of the occurrence of low-frequency vibration.

5. Conclusion and outlooks

The aim of this paper is to address three key questions: what is LFC, why is it challenging to predict with existing models, and how can we predict it? To answer these questions, a surface renewal (SR) model is proposed, which realizes the accurate calculation of the dynamic chip thickness and characterization of the modulated tool-workpiece engagement conditions. A non-parametric method for characterizing the dynamic characteristics based on impulse response function (IRF) is developed to account for mode coupling effects. Finally, an LFC stability model is established.

- Regarding what LFC is, the following conclusions can be drawn:
  1. LFC is a self-excited vibration caused by excited structural modes during robotic milling.
  2. The machining process shows the instability of the entire robot structure.
  3. The vibration spectrum shows a distinct low-frequency component.
  4. The occurrence of LFC (lobe order <1) is accompanied by a sideband frequency modulation phenomenon.
  5. LFC can occur in both high-speed regions with a lobe order <1 and low-speed regions with a lobe order ≥ 1.
- Regarding why existing models are unable to accurately predict LFC, the following conclusions can be drawn:
  1. The LFC prediction model based on the regenerative chatter mechanism cannot accurately predict LFC when the lobe order is less than 1. This is because the modulated tool-workpiece engagement condition is not considered, and the change in dynamic chip thickness during the chatter period is not fully accounted for, resulting in significant errors in the calculation of dynamic cutting forces.
  2. The LFC prediction model based on the regenerative chatter mechanism can predict LFC when the lobe order is greater than or equal to 1, but the accuracy of the prediction is limited because the model does not consider the mode coupling effects.
  3. The LFC prediction model based on mode coupling mechanism is not effective in predicting LFC in robotic milling, regardless of whether the lobe order is less than 1 or greater than or equal to 1. This is because the model assumes a threading operation and cannot accurately characterize the dynamic chip thickness. Additionally, the stability boundary loses speed dependence and remains a horizontal straight line that does not vary with spindle speed across the entire speed range. However, such models can be useful in predicting mode coupling chatter in threading operations.
- Regarding how to predict LFC, the following conclusions can be drawn:
  1. Proper modeling of mode coupling effect is crucial as LFC depends on the robotic structural modes.
  2. The LFC in robotic milling must comply with the milling characteristics, and the instantaneous chip thickness depends not only on the current vibration but also on the vibration marks left by the previous tooth on the workpiece surface.

3. Non-parametric characterization of dynamic characteristics based on IRF can effectively reduce the complexity of modeling the mode coupling effect.
4. For LFC, the natural frequency of the robot structure is usually too low, and in most cases, the lobe order is less than 1. The influence of the modulated tool-workpiece engagement conditions on the stability boundary increases with an increase in spindle speed. Therefore, it is essential to use surface renewal (SR) to characterize the tool-workpiece engagement conditions geometrically, which is an efficient and necessary approach.

- Through simulations and experiments, the following conclusions can be drawn:
  1. Increasing spindle speed can reduce the occurrence of LFC to some extent since the excitation frequency, which is far away from the structural mode frequency, is less likely to excite the low-frequency mode.
  2. Spectrum signals observation is an effective way to identify LFC in the low-speed region (lobe order ≥ 1). The workpiece surface is affected by low-frequency forced vibration, making it challenging to distinguish chatter from a stable state.
  3. In the high-speed region (lobe order <1), determining whether LFC occurs is easy through observation of sideband frequency signals. It is also possible to observe vibration marks on the workpiece's surface.
  4. Testing the 3D surface morphology of the workpiece can easily distinguish the effects of LFC and forced vibration on the workpiece surface in the high-speed region. Some analysis and research can be conducted based on this.
  5. LFC, similar to high-frequency chatter, also has significant speed dependence, which cannot be ignored in process parameter optimization.
  6. The sideband phenomenon is a modulation phenomenon of the low-frequency vibration signal with tooth-passing frequencies, rotation frequencies, and their multiples. The sideband signal appears with the occurrence of low-frequency vibration and can be used as a characteristic signal to determine whether LFC occurs.

Based on the above conclusions, future work can be categorized into three points. First, the stability constraint equation should be established to realize the robotic posture optimization based on the proposed method. Second, the dominant mode of the robotic LFC must be monitored online according to the characteristics of the sideband frequency. Finally, the development of suppression equipment around the robotic joint structure based on the characteristics of LFC is also important.

CRediT authorship contribution statement

Shihao Xin: Writing – review & editing, Writing – original draft, Visualization, Validation, Software, Methodology, Investigation, Data curation, Conceptualization. **Xiaowei Tang:** Writing – review & editing, Supervision, Resources, Project administration, Funding acquisition, Conceptualization. **Jiawei Wu:** Validation, Software, Investigation, Formal analysis. **Fangyu Peng:** Writing – review & editing, Supervision, Resources, Project administration, Funding acquisition. **Rong Yan:** Supervision, Resources, Project administration, Funding acquisition. **Wei Yang:** Visualization, Validation, Data curation.

Declaration of competing interest

The authors declare that they have no known competing financial interests or personal relationships that could have appeared to influence the work reported in this paper.

Data availability

No data was used for the research described in the article.

Acknowledgements

This research is supported by the National Natural Science Foundation of China under Grant No. 52175463, National Natural Science Foundation of China under Grant No. U20A20294, the Fundamental Research Funds for the Central Universities No. 2020kfyXJJS066, and National Natural Science Foundation of China under Grant No. 52188102.

Appendix A

Table A
1 Modal parameters of robotic structure for illustration.

Mode	Frequency (Hz)	Damping (%)	Residue
H_{xx}	15.88	3.34	−2.6540E-06 – 1.0224E-05j
H_{yx}			−3.4325E-06 – 6.9717E-06j
H_{zx}			−3.0120E-06 – 2.3183E-05j
H_{xy}	15.86	2.58	−3.2775E-06 – 1.0846E-05j
H_{yy}			−9.7594E-07 – 2.3137E-06j
H_{zy}			−1.6663E-06 – 9.7307E-06j
H_{xz}	15.92	1.86	−2.9478E-06 – 7.8039E-06j
H_{yz}			−4.4165E-07 – 1.5553E-06j
H_{zz}			−1.3210E-06 – 9.9552E-07j

References

[1] L. Yuan, Z. Pan, D. Ding, S. Sun, W. Li, A review on chatter in robotic machining process regarding both regenerative and mode coupling mechanism, IEEE ASME Trans. Mechatron. 23 (2018) 2240–2251.
[2] L.T. Tunc, D. Stoddart, Tool path pattern and feed direction selection in robotic milling for increased chatter-free material removal rate, Int. J. Adv. Manuf. Technol. 89 (2017) 2907–2918.
[3] Z.X. Pan, H. Zhang, Z.Q. Zhu, J.J. Wang, Chatter analysis of robotic machining process, J. Mater. Process. Technol. 173 (2006) 301–309.
[4] S.A. Tobias, W.J.E. Fishwick, Theory of regenerative machine tool chatter, The Engineer 205 (1958) 199–203.
[5] O. Gienke, Z. Pan, L. Yuan, T. Lepper, S. Van Duin, Mode coupling chatter prediction and avoidance in robotic machining process, Int. J. Adv. Manuf. Technol. 104 (2019) 2103–2116.
[6] L.T. Tunc, B. Gonul, Effect of quasi-static motion on the dynamics and stability of robotic milling, CIRP Ann.-Manuf. Technol. 70 (2021) 305–308.
[7] C. Chen, F. Peng, R. Yan, Z. Fan, Y. Li, D. Wei, Posture-dependent Stability Prediction of a Milling Industrial Robot Based on Inverse Distance Weighted Method, 28th International Conference on Flexible Automation and Intelligent

Manufacturing (FAIM) - Global Integration of Intelligent Manufacturing and Smart Industry for Good of Humanity, Columbus, OH, 2018, pp. 993–1000.
[8] M. Cordes, W. Hintze, Y. Altintas, Chatter stability in robotic milling, Robot. Comput.-Integr. Manuf. 55 (2019) 11–18.
[9] S. Mousavi, V. Gagnol, B.C. Bouzgarrou, P. Ray, Stability optimization in robotic milling through the control of functional redundancies, Robot. Comput.-Integr. Manuf. 50 (2018) 181–192.
[10] B. Gonul, O.F. Sapmaz, L.T. Tunc, Improved Stable Conditions in Robotic Milling by Kinematic Redundancy, 17th CIRP Conference on Modelling of Machining Operations, CIRP CMMO), AMRC, Sheffield, ENGLAND, 2019, pp. 485–490.
[11] C. Chen, F. Peng, R. Yan, X. Tang, Y. Li, Z. Fan, Rapid prediction of posture-dependent FRF of the tool tip in robotic milling, Robot. Comput.-Integr. Manuf. 64 (2020), 101906.
[12] J. Li, B. Li, N. Shen, H. Qian, Z. Guo, Effect of the cutter path and the workpiece clamping position on the stability of the robotic milling system, Int. J. Adv. Manuf. Technol. 89 (2017) 2919–2933.
[13] S.H. Xin, F.Y. Peng, C. Chen, X.W. Tang, R. Yan, Z.P. Li, J.W. Wu, Chip wave phase difference analysis of robotic milling and chatter dominant mode research, Int. J. Adv. Manuf. Technol. 122 (2022) 1431–1455.
[14] J. Munoa, X. Beudaert, Z. Dombovari, Y. Altintas, E. Budak, C. Brecher, G. Stepan, Chatter suppression techniques in metal cutting, CIRP Ann.-Manuf. Technol. 65 (2016) 785–808.
[15] Z.X. Pan, H. Zhang, Analysis and suppression of chatter in robotic machining process, in: International Conference on Control, Automation and Systems, SOUTH KOREA, Seoul, 2007, pp. 2874–2879.
[16] F.-X. He, L. Dai, Q. Chen, Y. Liu, Z. Luo, Three-dimensional stability analysis of robotic machining process, Ind. Robot 47 (2020) 82–89.
[17] L. Cen, S.N. Melkote, CCT-based mode coupling chatter avoidance in robotic milling, J. Manuf. Process. 29 (2017) 50–61.
[18] L. Cen, S.N. Melkote, J. Castle, H. Appelman, A method for mode coupling chatter detection and suppression in robotic milling, J. Manuf. Sci. Eng.-Trans. ASME 140 (2018), 081015.
[19] L.W. Wang, Y. Liu, Y. Yu, F.X. He, Research on reliability of mode coupling chatter of orthopedic surgery robot, Proc. Inst. Mech. Eng. Part C-J. Eng. Mech. Eng. Sci. 236 (2022) 8609–8620.
[20] Y. Liu, F. He, Study on the chatter stability of robotic milling based on the probability method, Journal of Northeastern University. Natural Science 40 (2019) 683–687.
[21] M. Maulimov, B. Sencer, Effect of Directional Relations on Milling Chatter Stability and Development of a Stability Index, 46th North American Manufacturing Research Conference (NAMRC), Texas A & M Univ, College Station, TX, 2018, pp. 372–382.
[22] Y. Liu, F. He, Research on the influencing factors of robot milling stability, Journal of Northeastern University. Natural Science 40 (2019) 991–996.
[23] H. Celikag, E. Ozturk, N.D. Sims, Can mode coupling chatter happen in milling? Int. J. Mach. Tool Manufact. 165 (2021), 103738.
[24] T. Insperger, B.P. Mann, G. Stépán, P.V. Bayly, Stability of up-milling and down-milling, part 1: alternative analytical methods, Int. J. Mach. Tool Manufact. 43 (2003) 25–34.
[25] A. Banerjee, H.Y. Feng, E.V. Bordatchev, Geometry of chip formation in circular end milling, Int. J. Adv. Manuf. Technol. 59 (2012) 21–35.
[26] S. Engin, Y. Altintas, Mechanics and dynamics of general milling cutters.: Part I: helical end mills, Int. J. Mach. Tool Manufact. 41 (2001) 2195–2212.
[27] M. Shi, X. Qin, H. Li, S. Shang, Y. Jin, T. Huang, Cutting force and chatter stability analysis for PKM-based helical milling operation, Int. J. Adv. Manuf. Technol. 111 (2020) 3207–3224.
[28] G. Totis, Breakthrough of regenerative chatter modeling in milling by including unexpected effects arising from tooling system deflection, Int. J. Adv. Manuf. Technol. 89 (2017) 2515–2534.
[29] S. Xin, F. Peng, X. Tang, R. Yan, Z. Li, J. Wu, Research on the influence of robot structural mode on regenerative chatter in milling and analysis of stability boundary improvement domain, Int. J. Mach. Tool Manufact. 179 (2022), 103918.
[30] L.M. Wang, Y.M. Shao, Z. Cao, Optimal demodulation subband selection for sun gear crack fault diagnosis in planetary gearbox, Measurement 125 (2018) 554–563.
[31] F. Koenigsberger, J. Tlusty, Machine Tool Structures, Machine tool structures, 1970.
[32] G. Totis, P. Albertelli, M. Sortino, M. Monno, Efficient evaluation of process stability in milling with spindle speed variation by using the Chebyshev collocation method, J. Sound Vib. 333 (2014) 646–668.
[33] G. Totis, T. Insperger, M. Sortino, G. Stépán, Symmetry breaking in milling dynamics, Int. J. Mach. Tool Manufact. 139 (2019) 37–59.
[34] D. Ewins, Modal Testing, Theory, Practice and Application, 1985.
[35] E. Kuljanic, M. Sortino, G. Totis, Multisensor approaches for chatter detection in milling, J. Sound Vib. 312 (2008) 672–693.
[36] Y. Altintas, Manufacturing Automation : Metal Cutting Mechanics, Machine Tool Vibrations, and CNC Design/2nd, Manufacturing Automation : Metal Cutting Mechanics, Machine Tool Vibrations, CNC design/2nd, 2012.
[37] N.D. Sims, Multi-frequency chatter analysis using the shift theorem, Procedia IUTAM 22 (2017) 3–9.
[38] G. Tu, X. Dong, C. Qian, S. Chen, L. Hu, Z. Peng, Intra-wave modulations in milling processes, Int. J. Mach. Tool Manufact. 163 (2021), 103705.